On the Dissociation of Aromatic Radical Anions in Solution. 2. Reaction Path and Rate Constant Analysis

Irene Burghardt,[†] Damien Laage,[‡] and James T. Hynes*[,‡,§]

Département de Chimie, CNRS UMR 8642, Ecole Normale Supérieure, 24 rue Lhomond, 75231 Paris Cedex 05, France, Département de Chimie, CNRS UMR 8640 PASTEUR, Ecole Normale Supérieure, 24 rue Lhomond, 75231 Paris Cedex 05, France, and Department of Chemistry and Biochemistry, University of Colorado, Boulder, Colorado 80309-0215

Received: June 10, 2003; In Final Form: September 26, 2003

The theoretical formulation presented for the solution reaction path and rate constant for the radical anion $[CN-\Phi-Cl]\bullet^-$ dissociation in solution, described in the preceding paper of this series of work, hereafter referenced as I. The reaction paths that lead to the bent geometry transition state, which is required for the avoidance of the conical intersection point, and cross through such a state vary with the solvent (e.g., water versus acetonitrile) and differ considerably from an equilibrium solvation image. A transition state theory (TST) rate constant, k_{TST}, is described in terms of reactive and nonreactive normal modes and is contrasted with a conventional equilibrium solvation perspective. Finally, dissipative frictional effects on the reaction rate are examined and determined to be negligible, which supports the use of the k_{TST} formula for the rate constant evaluation in I.

1. Introduction

In this paper, we examine the theoretical construction and calculation of the reaction paths and the rate constants for the dissociation of the radical anion $[CN-\Phi-Cl]\bullet^-$ in solution, which is a ground electronic state conical intersection reaction, the aspects of which have been analyzed in the first paper of this series of work[1] (hereafter referenced as I). Several of the numerical results that are developed within have already been used in I.

Our basic approach is in terms of a Hamiltonian formulation. This formulation can be then used to analyze the reaction path and rate constant, as shown by Lee and Hynes,[2] in a manner somewhat similar to a gas-phase reaction problem, except that (i) there is a free energy function *G*, rather than simply a potential energy function, and (ii) there is a solvent coordinate *s* in the description, which is, of course, critical. The reaction path, which is the solution phase analogue[2] of the gas-phase Fukui intrinsic reaction coordinate,[3] provides a molecular level picture (at least in the reacting solute) of the key motions involved on the way to the reaction transition state, the sequence in which they occur, and the motions that the reaction system uses to reach and cross the transition state. We have already emphasized in I that there must be a bending of the CCl, to avoid the conical intersection point as the C−Cl bond stretches. In the solvent dielectric continuum description that has been used, the participation of the solvent orientational polarization in the reaction path and transition-state crossing is revealed. In short, the reaction path is a picture of the mechanism of the reaction, including the solvent's role.

These reaction paths can be quite different for different solvents, and they generally are quite different from the gas-phase path. In addition, they generally are quite different from those paths calculated under the most common assumption that is applied for solution reactions. This is the assumption of equilibrium solvation, in which, for the radical anion dissociation, the solvent would be imagined to be always equilibrated to the reacting solute at each value of the C−Cl separation *r* and the C−Cl wag angle θ. As shown within, for the radical anion, the solvent does not have sufficient time to equilibrate to the rapidly changing charge distribution of the dissociating anion, and, instead, the reaction path involves extensive nonequilibrium solvation.

The rate-constant formulation in this Hamiltonian perspective is also a solution analogue of gas-phase transition state theory (TST), which involves the reaction coordinate at the transition state, as well as nonreactive mode motions there, all in the three-dimensional (3D) space (with coordinates r, θ, s). This allows a simple and precise expression for the rate constant, such that its various trends with, for example, solvent polarity can be analyzed, as was done in I. This 3D TST approach is quite different conceptually from what is usually understood as TST in solution; the latter implicitly or explicitly involves the equilibrium solvation assumption, which, as noted previously and shown within, is not correct.

The aforementioned Hamiltonian description is a nondissipative one. It does not include any dissipative, "frictional" effects on any of the three coordinates. These frictional effects include, for example, (i) an explicit role of the dynamical solvation time in response to a changed charge distribution, as measured in time-dependent fluorescence Stokes shift measurements of solvation dynamics,[4] and (ii) any "viscosity" effects that dampen the motion of an ion such as Cl^- moving through a solvent. It is important to examine the possible role of these frictions on the rate constant. If they are significant, then the 3D TST rate constant will be in error, to some degree, and our estimates in I would have to be revised. Indeed, it has been suggested[5] that, in the presence of "moats", avoiding a conical intersection point (which is exactly the situation established in I for the radical

* Author to whom correspondence should be addressed. E-mail: hynes@chimie.ens.fr.
† Département de Chimie, CNRS UMR 8642, Ecole Normale Supérieure.
‡ Département de Chimie, CNRS UMR 8640 PASTEUR, Ecole Normale Supérieure.
§ University of Colorado.

10.1021/jp035638m CCC: $25.00
Published on Web 11/25/2003

anion dissociation), there will be strong frictional damping effects, inducing diffusive motion in the moats, with a resulting strong reduction of the rate constant. These questions can be explicitly examined for the $[CN-\Phi-Cl]\bullet^-$ system by application of the Grote−Hynes theory[6,7] for dynamical friction effects on reaction rates. This theory has been repeatedly shown to be accurate via molecular dynamics tests for realistic solution reactions (see, for example, the work of Bergsma et al.[8] and Hynes[9]), and it has also proved useful for experiments (see, for example, the work of Hynes,[9] Kim and Hynes,[10] and Changenet et al.[11]).

The outline of the remainder of this paper is as follows. In Section 2, we develop the (r, θ, s) kinetic energy expression, which, together with the free energy surface $G(r, \theta, s)$ developed in I, completes the Hamiltonian description. Section 3 begins with the introduction of normal modes to facilitate the discussion of the solution reaction path, followed by a detailed analysis of the calculated reaction paths in the (r, θ, s) coordinates for the $[CN-\Phi-Cl]\bullet^-$ dissociation in the three solvents. A strong contrast is made with the paths expected on the basis of conventional equilibrium solvation view. The theoretical formulation of the TST rate constant expressions implemented in I is presented in Section 4, and its interpretation in terms of reactive and nonreactive normal modes is given. The contrast is also made with the rate constants that would result from an equilibrium solvation perspective. Section 5 examines the issue of whether any serious corrections for the TST rate constants are necessary that are due to the influence of dissipative frictional forces acting on the (r, θ, s) coordinates. Brief concluding remarks are given in Section 6.

2. Reaction System Hamiltonian

We first briefly describe the Hamiltonian formulation that is associated with the free energy surface described in I. The Hamiltonian

$$H = K + G(r, \theta, s) \tag{2.1}$$

is the sum of a kinetic energy K and the free energy $G(r,\theta,s)$. In I, we have already extensively discussed the free energy surface in the variables of the bond stretch r, the CCl wag angle θ, and the solvent coordinate s,

$$G(r,\theta,s) = \frac{G^{B}(r,\theta,s) + G^{A}(r,\theta,s)}{2} - \frac{1}{2}\sqrt{(G^{A}(r,\theta,s) - G^{B}(r,\theta,s))^2 + 4(\beta(\theta))^2} \tag{2.2}$$

in terms of the diabatic state free energies $G^{B,A}(r,\theta,s)$ and the angle-dependent electronic coupling $\beta(\theta)$. The evolving ground adiabatic electronic wave function during the dissociation is

$$\Psi(r,\theta,s) = c^{B}(r,\theta,s)\Psi^{B}(r,\theta) + c^{A}(r,\theta,s)\Psi^{A}(r,\theta) \tag{2.3}$$

in terms of the diabatic bound ($^2B_1$) and dissociative ($^2A_1$) state wave functions, where the squared coefficients $(c^{B})^2$ and $(c^{A})^2$, which measure their respective contributions, are

$$(c^{B,A}(r,\theta,s))^2 = \frac{1}{2}\left(1 \pm \frac{G^{A}(r,\theta,s) - G^{B}(r,\theta,s)}{\sqrt{[G^{A}(r,\theta,s) - G^{B}(r,\theta,s)]^2 + 4(\beta(\theta))^2}}\right) \tag{2.4}$$

For convenience, we will specify the explicit forms of $G^{B,A}$ and β that have been developed in I later, in Section 2.2. To complete the Hamiltonian description, the kinetic energy that is to be added to the free energy $G(r,\theta,s)$ must be found.

In Section 4 of I,[1] we introduced an intermediate solvent coordinate z, such that the orientational polarization field $\boldsymbol{P}_{or}(\boldsymbol{x})$ at a location x in the solvent was represented during the reaction by

$$\boldsymbol{P}_{or}(\boldsymbol{x}) = (1 - z)\,\boldsymbol{P}^{B}_{or\,eq}(\boldsymbol{x}; r,\theta) + z\,\boldsymbol{P}^{A}_{or\,eq}(\boldsymbol{x}; r,\theta) \tag{2.5}$$

i.e., a linear combination of the equilibrium polarizations, appropriate to the charge distributions of the reacting anion system in its diabatic states: the bound $^2B_1$ state and the dissociative $^2A_1$ state (see Section 2.1 of I) with internal coordinate values r and θ. There, it was stated that the conversion to a new solvent coordinate s—which ultimately led, after some approximations, to the free energy form $G(r,\theta,s)$ (eq 4.17 of I)—was necessary to diagonalize the kinetic energy such that there is no kinetic dynamic coupling between s and the solute internal coordinates r and θ. Here, we discuss this transformation, which allows s to be treated as an independent dynamical variable.[12]

The kinetic energy K is given by

$$K(r,\theta,\boldsymbol{P}_{or}(\boldsymbol{x})) = \frac{1}{2}\mu_r\dot{r}^2 + \frac{1}{2}\mu_\theta(r)\dot{\theta}^2 + K_{or}(\dot{\boldsymbol{P}}_{or}(\boldsymbol{x})) \tag{2.6}$$

with the solvent polarization contribution being given by

$$K_{or}(\dot{\boldsymbol{P}}_{or}(\boldsymbol{x})) = \frac{1}{2}m_{so}\int \mathrm{d}\boldsymbol{x}\,(\dot{\boldsymbol{P}}_{or}(\boldsymbol{x}))^2 \tag{2.7}$$

where the dot indicates time differentiation and μ_r is the reduced mass of the radial Cl-ring separation, $\mu_\theta(r)$ is the mass for the bend (which is r-dependent, because of the moment arm of the Cl atom, with respect to the ring C atom), and m_{so} is the orientational polarization mass of the solvent:

$$m_{so} = \frac{1}{\omega_s^2}\frac{4\pi}{1 - (\epsilon_\infty/\epsilon)} \tag{2.8}$$

where ω_s^2 is a constant squared solvent frequency. The factor $1 - (\epsilon_\infty/\epsilon)$ in eq 2.8 reflects the fact that the velocity of the comparatively slow orientational polarization is involved, rather than the extremely rapid electronic polarization (characterized by ϵ_∞).

For the reaction problem, the equilibrium polarizations in eq 2.5 for $\boldsymbol{P}_{or}(\boldsymbol{x})$ generally are dependent on r and θ, and the polarization velocity $\dot{\boldsymbol{P}}_{or}$ has contributions from $\dot{z}$ and r and $\dot{\theta}$:

$$\dot{\boldsymbol{P}}_{or}(\boldsymbol{x}) = \dot{z}(\boldsymbol{P}^{A}_{or,eq}(\boldsymbol{x}; r,\theta) - \boldsymbol{P}^{B}_{or,eq}(\boldsymbol{x}; r,\theta)) + \dot{r}\left[(1 - z)\frac{\partial \boldsymbol{P}^{B}_{or,eq}(\boldsymbol{x}; r,\theta)}{\partial r} + z\frac{\partial \boldsymbol{P}^{A}_{or,eq}(\boldsymbol{x}; r,\theta)}{\partial r}\right] + \dot{\theta}\left[(1 - z)\frac{\partial \boldsymbol{P}^{B}_{or,eq}(\boldsymbol{x}; r,\theta)}{\partial \theta} + z\frac{\partial \boldsymbol{P}^{A}_{or,eq}(\boldsymbol{x}; r,\theta)}{\partial \theta}\right] \tag{2.9}$$

When this relation is inserted into eq 2.7 for K_{or}, various cross terms emerge, e.g., in $\dot{z}\dot{r}$ and $\dot{z}\dot{\theta}$, such that z cannot be regarded as an independent dynamical variable. A different solvent coordinate is required.

To proceed to find this coordinate, we make several approximations. First, we neglect the θ dependence of the equilibrium polarizations $\boldsymbol{P}^{B,A}_{or,eq}(\boldsymbol{x}; r,\theta)$. Indeed, the wagging motion does not change the solute charge distribution of the anion in the diabatic states much and induces only a small

change in the resulting electric field. Second, for the solute in the bound state $^2B_1$, we ignore the r dependence of $\boldsymbol{P}^{B}_{or,eq}(\boldsymbol{x}; r,\theta)$, because there is little charge on the Cl atom in this state and the solute electric field will change negligibly as the C−Cl bond is stretched. (In I, we ultimately made a similar approximation for the dissociative $^2A_1$ state (cf. Section 4.1.2); however, it is convenient to retain the r dependence of $\boldsymbol{P}^{A}_{or,eq}$ for the moment.) $\boldsymbol{P}^{B}_{or,eq}(\boldsymbol{x}; r,\theta)$ then may be always assigned its value at $r = r^{B}_{eq}$, which is the equilibrium position in the B-state.

With these approximations, eq 2.9 simplifies considerably to

$$\dot{\boldsymbol{P}}_{or}(\boldsymbol{x}) = \dot{z}(\boldsymbol{P}^{A}_{or,eq}(\boldsymbol{x}; r) - \boldsymbol{P}^{B}_{or,eq}(\boldsymbol{x}; r^{B}_{eq})) + \dot{r}z\frac{\partial \boldsymbol{P}^{A}_{or,eq}(\boldsymbol{x}; r)}{\partial r} \tag{2.10}$$

and the kinetic energy in eq 2.7 becomes

$$K_{or} = \frac{1}{2}m_s(r)\dot{z}^2 + \alpha(r,z)\,\dot{z}\dot{r} + \frac{1}{2}\beta(r,z)\dot{r}^2 \tag{2.11}$$

in which the r-dependent solvent mass $m_s(r)$ is

$$m_s(r) = m_{so}\int d\boldsymbol{x}\,(\boldsymbol{P}^{A}_{or,eq}(\boldsymbol{x}; r) - \boldsymbol{P}^{B}_{or,eq}(\boldsymbol{x}; r^{B}_{eq}))^2 \tag{2.12}$$

and the α and β factors are

$$\alpha(r,z) = m_{so}z\int d\boldsymbol{x}\frac{\partial \boldsymbol{P}^{A}_{or,eq}(\boldsymbol{x}; r)}{\partial r}(\boldsymbol{P}^{A}_{or,eq}(\boldsymbol{x}; r) - \boldsymbol{P}^{B}_{or,eq}(\boldsymbol{x}; r^{B}_{eq})) \tag{2.13}$$

$$\beta(r,z) = m_{so}z^2\int d\boldsymbol{x}\left(\frac{\partial \boldsymbol{P}^{A}_{or,eq}(\boldsymbol{x}; r)}{\partial r}\right)^2 \tag{2.14}$$

Next, by introducing a solvent force constant $k_s(r)$,

$$k_s(r) = \omega_s^2 m_s(r) \tag{2.15}$$

in which ω_s^2 is the constant square solvent frequency in eq 2.8, such that the r dependence of $k_s(r)$ is that of $m_s(r)$, we note, from eqs 2.12−2.14, that

$$\alpha(r) = \frac{1}{2\omega_s^2}\frac{dk_s(r)}{dr} \tag{2.16}$$

It can then be readily verified that, with the new solvent coordinate, which is defined by

$$s = z\sqrt{\frac{k_s(r)}{k_s^B}} \tag{2.17}$$

where $k_s^B = k_s\,(r = r^{B}_{eq})$ is the force constant evaluated at the $^2B_1$-state equilibrium value of r, the polarization kinetic energy (given in eq 2.11) is now diagonal:

$$K_{or} = \frac{k_s^B}{2\omega_s^2}\dot{s}^2 + \frac{1}{2}\dot{r}^2\left(\beta(r,s) - \frac{\alpha(r,s)^2}{m_s(r)}\right) \tag{2.18}$$

The polarization kinetic energy K_{or} (given in eq 2.18) is now characterized by a constant mass:

$$\mu_s = \frac{k_s^B}{\omega_s^2} \tag{2.19}$$

This solvent mass μ_s enters in the solvent coordinate kinetic energy in eq 2.18 and is associated with eq 2.6, in regard to the total kinetic energy K, giving a renormalization contribution to the mass μ_r for the r coordinate. However, in the approximations developed in I (see Section 4.1.2 of I), the equilibrium orientation polarization $\boldsymbol{P}^{A}_{or,eq}$ is assumed to be independent of the stretching dissociative coordinate r. Thus, its derivative in both eqs 2.13 and 2.14 vanishes, with the consequence that $\alpha = \beta = 0$, and there is no renormalization of the r mass.

Thus, the final expression for the full kinetic energy is

$$K = \frac{1}{2}\mu_r\dot{r}^2 + \frac{1}{2}\mu_\theta(r)\dot{\theta}^2 + \frac{1}{2}\mu_s\dot{s}^2 \tag{2.20}$$

and the desired Hamiltonian description for the dissociating anion system in solution is

$$H = K + G(r,\theta,s) \tag{2.21}$$

with K being given by eq 2.21 and G being given by eq 2.2, with its components to be given explicitly in Section 2.2.

2.1. Solvent Mass and Inertial Solvation Dynamics. The constant solvent mass (given in eq 2.19) is directly related to the solvent frequency ω_s and the constant solvent force constant k_s^B. The latter is given in our analytical model by the second derivative of the diabatic free energy G^B, evaluated at the equilibrium bond extension r^{B}_{eq}:

$$k_s^B = \left.\frac{\partial^2 G^B}{\partial s^2}\right|_{r^{B}_{eq}} \tag{2.22}$$

However, one can show that the constant solvent mass μ_s is also given by the dielectric continuum expression in eq 2.8; there, it is called m_{so}. By combining eqs 2.19 and 2.22, we can determine the solvent frequency, and, thus, the solvent mass, by a more convenient route than using the dielectric continuum solvent mass expression in eq 2.8. This route is to use experimental time-dependent fluorescence Stokes shifts, i.e., time-dependent solvation dynamics, as was done in ref 10. The connection is the following. Carter and Hynes[13] (also see the work of Maroncelli[14]) have shown that the short-time, "inertial" component of the solvation dynamics is governed by the Gaussian function

$$\text{Inertial component} = \exp\left(-\frac{\omega_s^2 t^2}{2}\right) \tag{2.23}$$

thus providing ω_s (see Table 1). As discussed in more detail in Sections 4 and 5, this inertial frequency is quite distinct from any frictional aspects that are associated with the solvent coordinate s and is, thus, precisely the quantity needed for the nondissipative Hamiltonian description.

2.2. Free Energy Surface $G(r,\theta,s)$. The free energy surface $G(r,\theta,s)$ was developed in detail in I. Here, we gather together the explicit expressions for G and its ingredients to be used in the remainder of this paper. $G(r,\theta,s)$ is given by eq 2.2, in terms of the diabatic free energies $G^{B,A}$ and the coupling (eq 2.4 of I):

$$\beta(\theta) = b\theta \tag{2.24}$$

The final forms of $G^{B,A}$ are (eq 4.17 of I)

$$G^{B,A}(r,\theta,s) = V^{B,A}(r,\theta) + \Delta G^{B,A}_{s,eq} + \lambda_s(s - s^{B,A}_{eq}(r))^2 \quad (2.25)$$

in which $V^{B,A}(r,\theta)$ are the vacuum potentials (eq 2.6 in I)

$$V^B(r,\theta) = V^B_0 + D^B_e\{[1 - \exp[-a^B(r - r^B_{eq})]]\}^2 + \frac{1}{2}k_\theta\theta^2$$

$$V^A(r,\theta) = V^A_0 + D^A_e \exp(-a^A r) + \frac{1}{2}k_\theta\theta^2 \quad (2.26)$$

and where the equilibrium solvation free energies $\Delta G^{B,A}_s$ are given by (eq 4.32 of I, with the prime notation now suppressed)

$$\Delta G^B_{s,eq} = -\frac{\alpha}{2}\left(1 - \frac{1}{\epsilon}\right)\left(\frac{(q^B_{Cl})^2}{a_{Cl}} + \frac{(q^B_\Phi)^2}{a_\Phi} + \frac{2q^B_{Cl}q^B_\Phi}{d_{CC} + r^B_{eq}}\right)$$

$$\Delta G^A_{s,eq}(r) = -\frac{\alpha}{2}\left(1 - \frac{1}{\epsilon}\right)\left\{\frac{[q^A_{Cl}(r/\alpha)]^2}{a_{Cl}} + \frac{[q^A_\Phi(r/\alpha)]^2}{a_\Phi} + \frac{2q^A_{Cl}q^A_\Phi}{d_{CC} + r}\right\} \quad (2.27)$$

where α is the scaling parameter discussed in Section 4.2.2 of I and $q^{B,A}_{Cl}$ and $q^{B,A}_\Phi$ are the partial charges on the Cl atom and ring sites, in the $^2B_1$- and $^2A_1$-states, respectively. The equilibrium solvent coordinates $s^{B,A}_{eq}(r)$ for the $^2B_1$- and $^2A_1$-states entering in eq 2.25 were defined in I to be

$$s^B_{eq}(r) = 0$$

$$s^A_{eq}(r) = \sqrt{\frac{\lambda_s(r)}{\lambda_s(r^B_{eq})}} \quad (2.28)$$

The final nonequilibrium solvation term in eq 2.25 involves the reorganization energy λ_s and its r-dependent version $\lambda_s(r)$ (eq 4.36 of I with the prime notation suppressed):

$$\lambda_s = \alpha\left(\frac{1}{\epsilon_\infty} - \frac{1}{\epsilon}\right)\left\{\frac{[q^B_{Cl} - q^A_{Cl}(r^B_{eq})]^2}{2a_{Cl}} + \frac{[q^B_\Phi - q^A_\Phi(r^B_{eq})]^2}{2a_\Phi} + \frac{[q^B_{Cl} - q^A_{Cl}][q^B_\Phi - q^A_\Phi(r^B_{eq})]}{d_{CC} + r^B_{eq}}\right\}$$

$$\lambda_s(r) = \lambda_s(r = r^B_{eq}) \quad (2.29)$$

The latter enters the equilibrium value $s_{eq}(r,\theta)$ of the solvent coordinate for the adiabatic ground state (eq 4.20 of I), which can be rewritten as

$$s_{eq}(r,\theta) = (c^A_{eq}(r,\theta,s_{eq}))^2\sqrt{\frac{\lambda_s(r)}{\lambda_s}} \quad (2.30)$$

The squared A component of the electronic structure composition of the adiabatic wave function (eq 2.3), when the solvent is in equilibrium for a given (r,θ) set of coordinates for the radical anion, can be found via eq 2.4 and $\partial G/\partial s = 0$ for fixed r and θ.

3. Solution Reaction Path

Using eq 2.18 for the kinetic energy K and eqs 2.2 and 2.4−2.30 for the free energy surface and its ingredients, we can now calculate the radical anion reaction paths in solution in the 3-D space (r,θ,s). The reaction path is defined as a zero-kinetic-energy, mass-weighted, steepest-descent path from the transition state (TS) and toward either the reactant (R) or the product state.[2,15−19] On starting from R, the path describes how the reacting system reaches the TS, crosses it, and evolves thereafter. A useful terminology for the path is that it specifies the reaction coordinate. Before presenting the calculated paths in Section 3.2, we first discuss the concept of normal modes for the reaction, to help interpret those results.

TABLE 1: Solvent Static and High-Frequency Dielectric Constants (ϵ_0 and ϵ_∞, Respectively), Solvent Frequency (ω_s), and Solvation Time (τ_s)[a]

solvent	ϵ_0	ϵ_∞	ω_s (ps^{-1})	τ_s (ps)	μ_r (g/mol)	$\mu_\theta(r^\ddagger)$ (Å² g/mol)	μ_s (Å² g/mol)
water	78.4	1.7756	45	0.2	37.5	145	14
acetonitrile	37.5	1.7999	8.3	0.26	37.5	149	353
DMF	36.7	2.0398	7	2.0	37.5	148	426

[a] From ref 4; masses associated with the coordinates r, θ, s.

3.1. Normal-Mode Analysis. As noted in the Introduction, the solution reaction path (or reaction coordinate) is the condensed-phase analogue of the Fukui intrinsic reaction coordinate path in the gas phase.[3,20] It is also important to consider the directions transverse to this path. In the harmonic approximation at each point along the path, this will define nonreactive normal modes (NMs), i.e., stable modes of vibration perpendicular to the reaction path at that point. They are nonreactive modes, because it is the reaction path itself that the system follows from the R to the TS and beyond to effect the reaction. The identities and frequencies of these nonreactive NMs will generally vary along the reaction path, because the path composition in terms of r, θ, and s will vary, e.g., on going from the R to the TS.

The transverse nonreactive NMs and the reaction path coordinate—the reaction coordinate—are especially interesting in the R region and in the TS region. In the former region, these indicate how the reaction begins; in the latter region, they specify how the TS is crossed, which will be of special importance for us. In these two regions—which, as we will see, are sufficient to specify the reaction rate constant—in the harmonic approximation, the reaction coordinate itself becomes a NM: a reactive normal mode. In the R region, the reactive NM is a stable vibration, whereas at the TS, it is an unstable vibration, i.e., the reaction system is crossing the TS, "seeing" a parabolic free energy variation in the reaction coordinate direction. In this TS region, the transverse nonreactive NMs complete the picture of a saddle region. We now develop the description of all these modes and their frequencies.

3.1.1. Normal Mode Transformation. In the TS neighborhood, the first derivatives of the free energy $G(r,\theta,s)$ vanish, and the equations of motion are

$$\begin{cases} \ddot{\delta}r = -\frac{1}{\mu_r}G^\ddagger_{r,r}\,\delta r - \frac{1}{\sqrt{\mu_r\mu_\theta}}G^\ddagger_{r,\theta}\,\delta\theta - \frac{1}{\sqrt{\mu_r\mu_s}}G^\ddagger_{r,s}\,\delta s \\ \ddot{\delta}\theta = -\frac{1}{\sqrt{\mu_r\mu_\theta}}G^\ddagger_{r,\theta}\,\delta r - \frac{1}{\mu_\theta}G^\ddagger_{\theta,\theta}\,\delta\theta - \frac{1}{\sqrt{\mu_\theta\mu_s}}G^\ddagger_{\theta,s}\,\delta s \\ \ddot{\delta}s = -\frac{1}{\sqrt{\mu_r\mu_s}}G^\ddagger_{r,s}\,\delta r - \frac{1}{\sqrt{\mu_\theta\mu_s}}G^\ddagger_{\theta,s}\,\delta\theta - \frac{1}{\mu_s}G^\ddagger_{s,s}\,\delta s \end{cases} \quad (3.1)$$

The notation for the various free-energy second-derivative terms has been condensed into, for example, $G^\ddagger_{r\theta} = \partial^2 G/(\partial r\,\partial\theta)|_\ddagger$, and we have introduced the deviations of r, θ, and s from their TS values (e.g., $\delta r = r - r^\ddagger$). μ_r, μ_θ, and μ_s are the notations that we will use from this point forward for the respective masses of each coordinate. The θ coordinate associated mass (μ_θ) is evaluated at the TS geometry (see Table 1).

For both the NM analysis and the reaction-path calculations, we require mass- weighted coordinates: these are simply the usual coordinates r, θ, and s, scaled by the square root of the appropriate mass, $r' = \sqrt{\mu_r}r$; $\theta' = \sqrt{\mu_\theta}\theta$; $s' = \sqrt{\mu_s}s$. In all that follows, we will use the mass-weighted coordinates; therefore, we will suppress the prime symbols. However, we do retain the $G^{\ddagger}_{xy}$ notation, to indicate the free-energy derivatives, with respect to the unscaled coordinates.

The Hessian matrix that is associated with eq 3.1 can be diagonalized; i.e., one can find the rotation matrix $\mathbf{R}^{\ddagger}$ such that NM frequencies are generated:[21]

$$\begin{pmatrix} \omega_1^{\ddagger 2} & 0 & 0 \\ 0 & \omega_2^{\ddagger 2} & 0 \\ 0 & 0 & \omega_3^{\ddagger 2} \end{pmatrix} = \mathbf{R}^{\ddagger} \begin{pmatrix} -\frac{1}{\mu_r}G^{\ddagger}_{r,r} & -\frac{1}{\sqrt{\mu_r\mu_\theta}}G^{\ddagger}_{r,\theta} & -\frac{1}{\sqrt{\mu_r\mu_s}}G^{\ddagger}_{r,s} \\ -\frac{1}{\sqrt{\mu_r\mu_\theta}}G^{\ddagger}_{r,\theta} & -\frac{1}{\mu_\theta}G^{\ddagger}_{\theta,\theta} & -\frac{1}{\sqrt{\mu_\theta\mu_s}}G^{\ddagger}_{\theta,s} \\ -\frac{1}{\sqrt{\mu_r\mu_s}}G^{\ddagger}_{r,s} & -\frac{1}{\sqrt{\mu_\theta\mu_s}}G^{\ddagger}_{\theta,s} & -\frac{1}{\mu_s}G^{\ddagger}_{s,s} \end{pmatrix} (\mathbf{R}^{\ddagger})^{-1} \quad (3.2)$$

At the TS, the Hessian eigenvectors are the three mass-weighted NMs, which are linear combinations of the coordinates δr, $\delta\theta$, δs. Here, the topology of the free-energy surface corresponds to a saddle point: one mode—the reactive mode $x_1^{\ddagger}$—is unstable, whereas the two other modes, which are the transverse modes $x_2^{\ddagger}$ and $x_3^{\ddagger}$, are stable. These $x_i^{\ddagger}$ modes are defined, with respect to the (r, θ, s) coordinates, by the rotation matrix $\mathbf{R}^{\ddagger}$

$$\begin{pmatrix} x_1^{\ddagger} \\ x_2^{\ddagger} \\ x_3^{\ddagger} \end{pmatrix} = \mathbf{R}^{\ddagger} \begin{pmatrix} \delta r \\ \delta\theta \\ \delta s \end{pmatrix} \quad (3.3)$$

and the NM equations of motion are

$$\begin{cases} \ddot{x}_1^{\ddagger} = \omega_1^{\ddagger 2} x_1^{\ddagger} \\ \ddot{x}_2^{\ddagger} = -\omega_2^{\ddagger 2} x_2^{\ddagger} \\ \ddot{x}_3^{\ddagger} = -\omega_3^{\ddagger 2} x_3^{\ddagger} \end{cases} \quad (3.4)$$

A precisely similar analysis can be conducted in the R region, where the three stable NMs correspond to motion along the reaction coordinate direction there and the two transverse vibrations. The equations of motion are

$$\begin{cases} \ddot{x}_1^{R} = \omega_1^{R2} x_1^{R} \\ \ddot{x}_2^{R} = -\omega_2^{R2} x_2^{R} \\ \ddot{x}_3^{R} = -\omega_3^{R2} x_3^{R} \end{cases} \quad (3.5)$$

and the relation of these NMs to the original (mass-weighted) coordinates is

$$\begin{pmatrix} x_1^{R} \\ x_2^{R} \\ x_3^{R} \end{pmatrix} = \mathbf{R}^{R} \begin{pmatrix} \delta r \\ \delta\theta \\ \delta s \end{pmatrix} \quad (3.6)$$

where the $\mathbf{R}^{R}$ matrix is defined by the relation

$$\begin{pmatrix} \omega_1^{R2} & 0 & 0 \\ 0 & \omega_2^{R2} & 0 \\ 0 & 0 & \omega_3^{R2} \end{pmatrix} = \mathbf{R}^{R} \begin{pmatrix} -\frac{1}{\mu_r}G^{R}_{r,r} & -\frac{1}{\sqrt{\mu_r\mu_\theta}}G^{R}_{r,\theta} & -\frac{1}{\sqrt{\mu_r\mu_s}}G^{R}_{r,s} \\ -\frac{1}{\sqrt{\mu_r\mu_\theta}}G^{R}_{r,\theta} & -\frac{1}{\mu_\theta}G^{R}_{\theta,\theta} & -\frac{1}{\sqrt{\mu_\theta\mu_s}}G^{R}_{\theta,s} \\ -\frac{1}{\sqrt{\mu_r\mu_s}}G^{R}_{r,s} & -\frac{1}{\sqrt{\mu_\theta\mu_s}}G^{R}_{\theta,s} & -\frac{1}{\mu_s}G^{R}_{s,s} \end{pmatrix} (\mathbf{R}^{R})^{-1} \quad (3.7)$$

and differs from the TS region matrix $\mathbf{R}^{\ddagger}$: the identity of the various NMs is generally different in the R and TS regions.

3.1.2. Origin of Coordinate Couplings for the NMs. It will be useful for our subsequent discussion to discuss the nature of the couplings between the coordinates that generate the various NMs, which result from the cross terms in the free-energy derivatives G_{xy}. For this purpose, it is convenient to use the free-energy surface expression in eq 2, in terms of the occupation probabilities $(c^B)^2$ and $(c^A)^2$ (eq 2.4) for the diabatic states $\Psi^{B,A}$ in the adiabatic wave function Ψ (see eq 2.3). The first derivative of G, with respect to any coordinate y, varies with the varying electronic structure, according to

$$\frac{\partial G}{\partial y} = (c^B)^2\frac{\partial G^B}{\partial y} + (c^A)^2\frac{\partial G^A}{\partial y} - 2c^B c^A\frac{\partial \beta}{\partial y} \quad (3.8)$$

where we have also used eq 2.4. This general expression for the gradients of G, which govern the reaction path itself, can be used to gain some insight on the G second-derivative factors that determine the NMs in the R and TS regions.

In the R region, $(c^B)^2 \simeq 1$ and $(c^A)^2 \simeq 0$; therefore, with eqs 2.25−2.27 for the diabatic free energies $G^{B,A}$ and eq 2.24 for the coupling β, we conclude that, in the R region,

$$\frac{\partial G}{\partial r} \simeq \frac{\partial V^B}{\partial r} = \text{a function of } r \text{ only}$$

$$\frac{\partial G}{\partial \theta} \simeq \frac{\partial V^B}{\partial \theta} = k_\theta\theta$$

$$\frac{\partial G}{\partial s} \simeq \frac{\partial V^B}{\partial s} = k_s s \quad (3.9)$$

so that there is negligible coupling between coordinates. Thus, the NMs will correspond to the coordinates (r, θ, s).

The situation is quite different in the TS region. There, the electronic structure is changing rapidly, $(c^B)^2 \simeq (c^A)^2$ and are rapidly varying with assorted coordinates (as we will see); thus, a coupling between the coordinates will result, such that the NMs will be various combinations of the basic (r,θ,s) coordinates NMs. Even in the special case of the wag angle, where the two first terms of eq 3.8 become independent of the electronic structure—because the derivatives $\partial G^{B,A}/\partial\theta = k_s\theta$ are equal and $(c^B)^2 + (c^A)^2 = 1$—the term that involves the derivative of the angle-dependent electronic coupling remains electronic structure-dependent,

$$\frac{\partial G}{\partial \theta} = k_s\theta - 2c^B c^A\frac{\partial \beta}{\partial \theta} \quad (3.10)$$

thus inducing, generally, a coupling between θ and the other coordinates via $c^B c^A$.

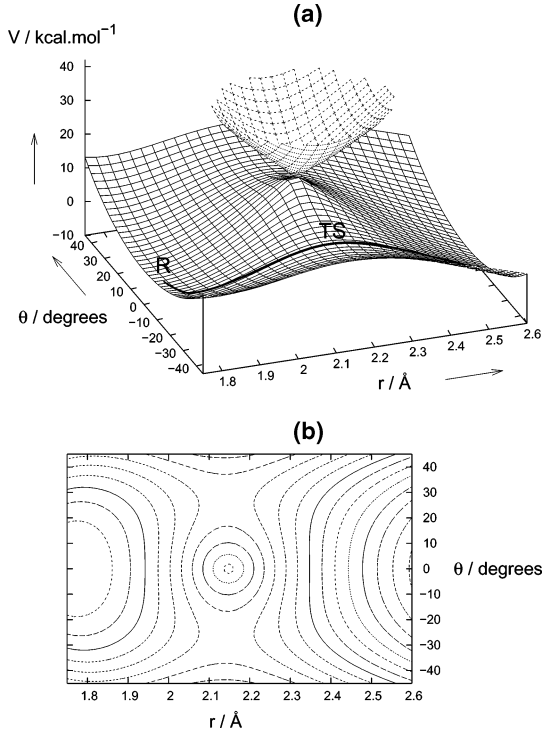

Figure 1. Gas-phase potential energy surface for [CN−Φ−Cl]•$^-$ with $k_\theta = 28$ cal/deg^2: (a) three-dimensional (3D) representation and (b) contour plot with a 2 kcal spacing between two successive contour lines. (Note that the actual well in θ for large r values should be softer in θ, because we assumed the k_θ force constant to be independent of r.)

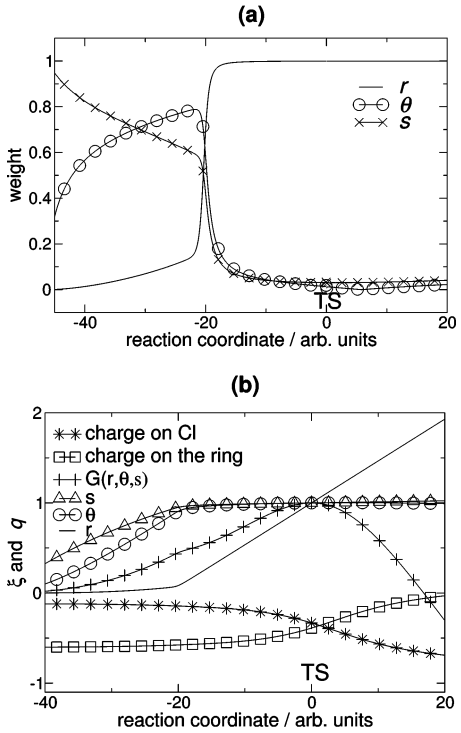

Figure 2. Dissociation of [CN−Φ−Cl]•$^-$ in dimethyl formamide (DMF) (case f in I): (a) contribution of each (mass-weighted) coordinate to the reaction coordinate along the reaction path; and (b) normed progress $\xi = x/x^\ddagger$ (with $x = r, \theta, s, G$) of the three coordinates and of the free energy, together with the charges on the ring and Cl sites, along the reaction path.

3.2. Reaction Path. We now turn to the calculation of the [CN−Φ−Cl]•$^-$ dissociation reaction paths in the three solvents: water, acetonitrile, and dimethyl formamide (DMF). The results for acetonitrile are very similar to those of DMF; therefore, we do not present explicit results for it.

To calculate the reaction path, the first step is to locate the TS on the reactive surface, which is accomplished in a standard fashion. Topologically, the TS is a saddle point; i.e., all the free-energy first derivatives, with respect to the different coordinates, are zero, and it is a minimum along all coordinates except one. After the TS has been located, two trajectories are calculated, both of which start along the unstable mode but in opposite directions: one leads to the reactant and the other to the product. Each trajectory is calculated as a zero-kinetic-energy, mass-weighted, steepest-descent path from the TS and toward either the reactant or the product state.

The reaction path is determined on the G surface with three coordinates (r, θ, s); therefore, it is difficult to plot it in any intuitive way. To address this situation, we will present the calculated contribution of each of the three coordinates to the reaction coordinate, i.e., the contribution to the reaction path. We supplement this with calculations of the various reactive and nonreactive NM frequencies in the R region and at the TS to give some further insight.

It is useful, for perspective, to first recall the potential energy surface for the dissociation in a vacuum (see Figure 4 of I), reproduced here for convenience as Figure 1.[22] The basic character of the reaction path is obvious from this figure: starting from R, the CCl angle will first bend to avoid the conical intersection point, followed by significant motion in the CCl stretch, which is the reaction coordinate at the bent TS.

Figure 2 shows the calculated results for the anion dissociation in the DMF solvent. Panel (a) shows that, starting from the R region, the solvent begins to reorganize first, and then the wag angle starts to change, again so that the conical intersection point will eventually be avoided, and ultimately the CCl bond stretches; the reaction coordinate at the bent TS is almost exclusively the bond stretch, just as it is in the vacuum (see Figure 1). These basic characteristics are also displayed in a different way in Figure 2b, where the progress of the system free energy is also shown.

TABLE 2: Frequencies in the Reactant along the Coordinates *r, θ, s,* Normal-Mode Frequencies in the Reactant (R) and at the Transition State (TS), and Activation Free Energy ($\Delta G^\ddagger$) in the Three Solvents[a]

	water (case a)	MeCN (case e)	DMF (case f)
ω_r^R (ps^{-1})	74	74	74
ω_θ^R (ps^{-1})	10	10	10
ω_s^R (ps^{-1})	45	8	7
$\omega_{\|\|}^R$ (ps^{-1})	10	8	7
$\omega_{\perp 1}^R$ (ps^{-1})	45	10	10
$\omega_{\perp 2}^R$ (ps^{-1})	74	74	74
$\omega_{\|\|}^\ddagger$ (ps^{-1})	75	70	70
$\omega_{\perp 1}^\ddagger$ (ps^{-1})	14	14	14
$\omega_{\perp 2}^\ddagger$ (ps^{-1})	46	9	8
$\Delta G^\ddagger$ (kcal/mol)	9.7	10.2	9.9

[a] See eq 4.3.

Important general aspects of this path follow from a consideration of characteristic time scales, determined by the inverse of the frequencies that are associated with coordinate motions. In the R region, the coordinate frequencies are given in Table 2 in the DMF solvent; these also coincide with the R-region NM frequencies, as is to be expected from our discussion in

Section 3.1, which indicates small coupling between the coordinates r, θ, and s. On the basis of these frequencies, in the DMF solvent, the solvent coordinate is the slowest, followed by the angle and the bond stretch, which is, by far, the fastest coordinate. This, of course, is consistent with the time sequence pattern of Figure 2 when one realizes that to ultimately cross the TS, which is a rapid process, slow coordinates must reorganize first; there will be no time to do this in the TS passage itself. Of course, the frequency values used for this argument were those in the R region, and this is not the complete story. Electronic structure variation issues are also key, as implied by our discussion in Section 3.1 and now discussed.

Figure 2b shows the radical anion electronic structure variation along the reaction path in DMF as the charge is adiabatically transferred from the ring (designated by Φ) to the Cl atom. This information is presented in terms of the charges associated with the adiabatic wave function Ψ (from eq 2.3) along the reaction path:

$$q_\Phi = (c^B)^2 q_\Phi^B + (c^A)^2 q_\Phi^A$$

$$q_{Cl} = (c^B)^2 q_{Cl}^B + (c^A)^2 q_{Cl}^A$$

$$q_\Phi^B = -0.60$$

$$q_\Phi^A(r) = 0.28 - 3.2 \exp\left(-\frac{r}{0.9\ \text{Å}}\right)$$

$$q_{Cl}^B = -0.12$$

$$q_{Cl}^A(r) = -1 + 3.2 \exp\left(-\frac{r}{0.9\ \text{Å}}\right) \qquad (3.11)$$

In approximately half of the progress displayed from the R to the TS, the electronic structure remains essentially that of the R, and the aforementioned frequency arguments still apply. Figure 2b shows that most of the electronic structure variation is concentrated in the TS neighborhood, and that, very importantly, the changes that s and θ are going to make on the way to the TS are *already* completed. The solvent coordinate has preorganized to be appropriate to the approximately 50/50 charge distribution at the TS *before* that charge distribution is established, and the wag angle has increased to provide the electronic coupling, allowing that charge distribution (and, of course, avoiding the conical intersection point). As the system heads into the neighborhood of the TS, s and θ are no longer involved, leaving only the most rapid coordinate r: notice in Figure 2a that, in the region of rapid increase in contribution of r to the reaction coordinate, s and θ drop out rapidly. The fact that the basic ordering of time scales still applies in the TS region is further confirmed by examination of the NM frequencies at the TS (see Table 2). The highest of these, the parallel frequency $\omega_{||}^{\ddagger}$, is obviously mainly associated with the bond stretch r, though now this is an unstable motion in the barrier region. The frequencies of the two transverse modes $\omega_{\perp 1}^{\ddagger}$ and $\omega_{\perp 2}^{\ddagger}$, which are essentially the angle and the solvent respectively, both have frequencies lower than that of r, and are again in the order angle higher than solvent.

As noted previously, the picture for the reaction in acetonitrile is essentially the same as that in DMF, as should be evident from the comparison of their characteristic frequencies in Table 2.

For the $[CN-\Phi-Cl]\bullet^-$ dissociation in the water solvent, however, the reaction path is noticeably different (see Figure 3). Panel (a) shows that the initial motion away from the R region is in the wag angle. The solvent then rearranges somewhat, the C−Cl bond stretches, and the TS is crossed along a mixture of the bond stretch and solvent coordinates. This is not only in significant contrast to the DMF case, but it also contrasts with the vacuum reaction in the identity of the TS reaction coordinate.

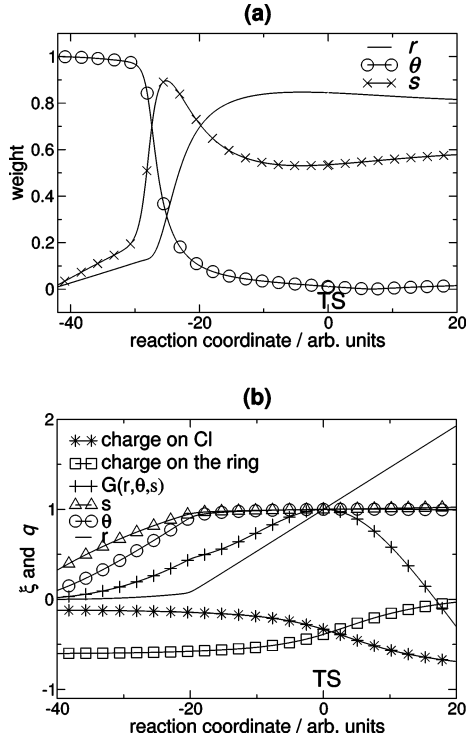

Figure 3. Dissociation of $[CN-\Phi-Cl]\bullet^-$ in water (case a in I): (a) contribution of each (mass-weighted) coordinate to the reaction coordinate along the reaction path; and (b) normed progress $\xi = x/x^{\ddagger}$ (with $x = r, \theta, s, G$) of the three coordinates and of the free energy, together with the charges on the ring and Cl sites, along the reaction path.

Again, time-scale considerations are critical here. The frequency entries in Table 2 for the R region show that, in water, the solvent is much faster than the wag angle (the opposite of the DMF situation) and is, in turn, slower than the bond stretch, which accounts for the basic ordering of the motions in Figure 3a. The fast time-scale character of water, which is directly reflected in the very short inertial time scale ($\simeq\omega_s^{-1}$) that is observed experimentally, results from the water librational (hindered rotational) motions. The librational motions of the light H atoms have a high frequency, and, therefore, the water dipole moments can rearrange very quickly; in the present continuum description, the water orientational polarization can adjust rapidly.

Beyond the feature that the wag angle is the slowest coordinate for the reaction in water, its central role in establishing the electronic coupling and avoiding the conical intersection point is much the same as that in DMF, and we do not consider it further. The continued significant involvement of the solvent coordinate in the reaction coordinate motion all the way to the bent TS is striking (Figure 3a). This aspect is also associated with the rapidity of the water motions. Although not as fast as the r-coordinate, the water solvent coordinate is sufficiently fast to at least partially adjust to the changing electronic structure and charge distribution as the reaction proceeds (Figure 3b). Finally, the fact that the ordering of the time scales we have used in our discussion remains the same in the TS region is

TABLE 3: Frequencies in the Reactant along the *r*, *θ*, *s* Coordinates, Normal-Mode Frequencies in the Reactant (R) and at the Transition State (TS), in the Three Solvents, in the ES Picture[a]

	water (case a)	MeCN (case e)	DMF (case f)
$\omega^{R}_{r,ES}$ (ps^{-1})	74	74	74
$\omega^{R}_{\theta,ES}$ (ps^{-1})	10	10	10
$\omega^{R}_{s,ES}$ (ps^{-1})	45	8	7
$\omega^{R}_{\|\|,ES}$ (ps^{-1})	10	10	10
$\omega^{R}_{\perp,ES}$ (ps^{-1})	74	74	74
$\omega^{R}_{s,ES}$ (ps^{-1})	45	8	7
$\omega^{\ddagger}_{\|\|,ES}$ (ps^{-1})	97	92	89
$\omega^{\ddagger}_{\perp,ES}$ (ps^{-1})	14	14	14
$\omega^{\ddagger}_{s,ES}$ (ps^{-1})	36	7	6

[a] See eq 4.10.

confirmed by the TS reactive and transverse nonreactive NM frequencies in Table 2.

3.3. Equilibrium Solvation Reaction Path. We can compare the reaction paths just discussed with those that would follow from the most common view of chemical reactions in solution. The latter adopts a different view from that previously used, in that an equilibrium solvation (ES) perspective is assumed: the solvent is considered to be always equilibrated, at each value of the reacting molecule coordinates. This is also the assumption of various calculational methods that involve quantum chemistry in solution[23] and has been used in some studies of radical anion dissociation.[24]

For the anion dissociation, the equilibrium solvent coordinate s_{eq} for a given molecular geometry is defined such that the free energy is minimized at each point of the (r,θ) surface,

$$\left.\frac{\partial G(r,\theta,s)}{\partial s}\right|_{r,\theta,s_{eq}} = 0 \qquad (3.12)$$

such that the solvent coordinate, which is defined as a function $s_{eq}(r,\theta)$ of the remaining coordinates, is then a nonreactive transverse coordinate.

To calculate the reaction path in the ES perspective, we use the same NM analysis as that used previously, where the solvent coordinate was explicit, with the exception that only the *r* and *θ* modes remain, the solvent coordinate always being a transverse, nonreactive coordinate. The counterpart of eq 3.3 is

$$\begin{pmatrix} x^{\ddagger}_{1,ES} \\ x^{\ddagger}_{2,ES} \end{pmatrix} = \mathbf{R}^{\ddagger}_{ES} \begin{pmatrix} \delta r \\ \delta\theta \end{pmatrix} \qquad (3.13)$$

The comparison of the reaction coordinate frequencies in the full 3D picture and in the equilibrium solvation approach shows that the ES picture strongly sharpens the apparent barrier. Thus, for example, from Tables 2 and 3, the barrier frequency $\omega^{\ddagger}_{||}$ in water is 75 ps^{-1} in the 3D picture, whereas in the ES description, there is a marked increase to a value of $\omega^{\ddagger}_{||,ES} = 97$ ps^{-1}. This effect is due to the very rapid change in the solvent coordinate around the barrier, which, in the ES description, must "instantly" equilibrate to the rapidly changing charge distribution. This can be observed, for example, in the approach to the TS in Figure 4b. The charges on the two sites change very rapidly, and, in the ES picture, the solvent instantly adapts to the evolving charge distribution. In particular, the change in solvent coordinate (s_{eq}) is restricted to the immediate neighborhood of the TS, where

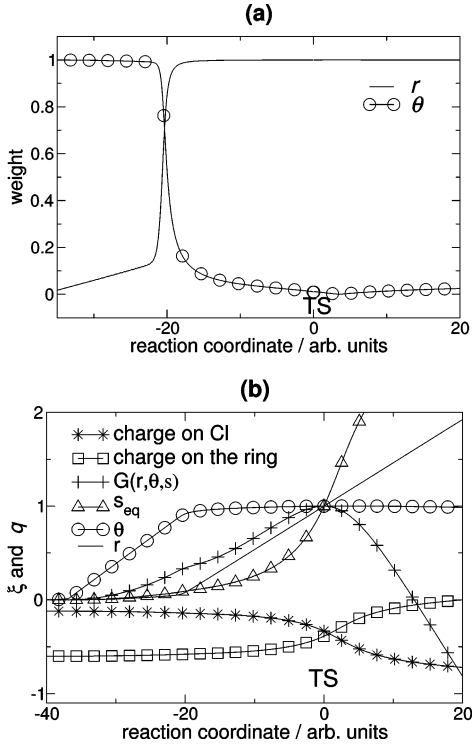

Figure 4. Dissociation of $[CN-\Phi-Cl]^{\bullet-}$ in water (case a in I) in the ES picture: (a) contribution of each (mass-weighted) coordinate to the reaction coordinate along the reaction path; and (b) normed progress $\xi = x/x^{\ddagger}$ (with $x = r$, θ, s_{eq}, G) of the three coordinates and of the free energy, together with the charges on the ring and Cl sites, along the ES reaction path.

the charges change rapidly. In contrast, along the correct reaction path (Figure 2), considerable solvent rearrangement has occurred long before the TS region is reached, and the solvent coordinate motion in the TS region itself is far less.

There is a remaining important comparison to make: the ES reaction paths for reaction in DMF and water in Figure 5a and 4a, versus the full paths for these two solvents in Figure 5b and 4b. For the ES description, the two paths are very similar to each other, with very small differences that are due only to the different dielectric constants of the two solvents; the dynamical properties of the solvents have no role, because the solvent is assumed to be instantly equilibrated. In strong contrast, the true reaction paths (with the explicit solvent coordinate) differ quite considerably for the two solvents, reflecting their important dynamical differences.

4. Transition State Theory Rate Constants

4.1. Rate Constant. We now present and discuss the radical anion dissociation rate constant in solution, using transition state theory (TST) and the normal-mode (NM) perspective that we introduced in Section 3.1. Although the result can be derived from flux time correlation formulas,[6,7] we follow a simpler route here.

The standard TST rate-constant formula[25] for a unimolecular reaction such as the present one is adapted for our free-energy surface:

$$k_{TST} = 2\left(\frac{k_B T}{\hbar}\right)\left(\frac{Q^{\ddagger}}{Q^{R}}\right)\exp\left(-\frac{\Delta G^{\ddagger}}{RT}\right) \qquad (4.1)$$

in which $\hbar$ is Planck's constant, $Q^{\ddagger}$ is the partition function (pf) of the TS species, Q^{R} is the pf of **R**, and $\Delta G^{\ddagger}$ is the activation free energy, i.e., the free energy of the TS species

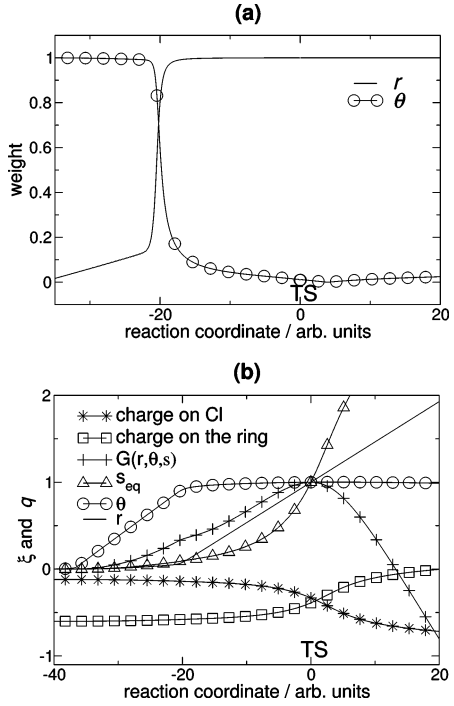

Figure 5. Dissociation of $[CN-\Phi-Cl]^{\bullet-}$ in DMF (case e in I) in the ES picture: (a) contribution of each (mass-weighted) coordinate to the reaction coordinate along the reaction path; and (b) normed progress $\xi = x/x^{\ddagger}$ (with $x = r$, θ, s_{eq}, G) of the three coordinates and of the free energy, together with the charges on the ring and Cl sites, along the ES reaction path.

minus the free energy of **R**. We include the symmetry factor of 2, because of the two routes around the conical intersection, with symmetrically related but otherwise identical TSs. We first need to stress a point that was made as an example in the Introduction, that our G has free-energy character, rather than strictly potential-energy character, because of the fact that all the molecular solvent degrees of freedom have been collapsed to the single solvent coordinate. (Thus, for a given value of s, many different microscopic solvent molecule configurations are possible.) However, otherwise, it acts precisely as a potential energy, from the point of view of the system Hamiltonian, the reaction path, and the rate constant. Thus, $\Delta G^{\ddagger}$ in eq 1 is directly analogous to the potential energy difference between the TS and the R in a gas-phase reaction (or, indeed, the vacuum radical anion dissociation).

With this concept being understood, the meaning of $Q^{\ddagger}$ is that it is the pf of the system fixed at the TS value of the reaction coordinate and, thus, exclusively involves the transverse nonreactive coordinate motions at the TS. In the 3D NM perspective, these are the two transverse vibrations with respective frequencies $\omega_{\perp 1}^{\ddagger}$, $\omega_{\perp 2}^{\ddagger}$, with each individual mode having its own vibration pf $q_{\perp 1}^{\ddagger}$, $q_{\perp 2}^{\ddagger}$. In the R region, there are three NM vibrations—one parallel to the reaction coordinate, and two transverse—with frequencies $\omega_{||}^{R}$ and $\omega_{\perp 1}^{R}$, $\omega_{\perp 2}^{R}$, respectively, and each mode has a vibrational pf. Given these considerations, eq 4.1 becomes

$$k_{TST} = 2\frac{k_B T}{\hbar}\frac{1}{q_{||}^{R}}\frac{q_{\perp 1}^{\ddagger} q_{\perp 2}^{\ddagger}}{q_{\perp 1}^{R} q_{\perp 2}^{R}}\exp\left(-\frac{\Delta G^{\ddagger}}{RT}\right) \tag{4.2}$$

In the classical approximation for the various vibrations, each vibrational pf q term is[26] $q = k_B T/(\hbar\omega)$, so that we obtain

$$k_{TST} = 2\left(\frac{\omega_{||}^{R}}{2\pi}\right)\left(\frac{\omega_{\perp 1}^{R}}{\omega_{\perp 1}^{\ddagger}}\right)\left(\frac{\omega_{\perp 2}^{R}}{\omega_{\perp 2}^{\ddagger}}\right)\exp\left(-\frac{\Delta G^{\ddagger}}{RT}\right) \tag{4.3}$$

which is independent of Planck's constant $\hbar$, as it should be. This is the formula used in I to calculate the dissociation rate constants in three solvents. The prefactor A_{sol} of the exponential in k_{TST} introduced in I is just

$$A_{sol} = 2\left(\frac{\omega_{||}^{R}}{2\pi}\right)\left(\frac{\omega_{\perp 1}^{R}}{\omega_{\perp 1}^{\ddagger}}\right)\left(\frac{\omega_{\perp 2}^{R}}{\omega_{\perp 2}^{\ddagger}}\right) \tag{4.4}$$

It is worthwhile to express eq 4.3 in a different way:

$$k_{TST} = 2\left(\frac{\omega_{||}^{R}}{2\pi}\right)\exp\left(\frac{\Delta S^{\ddagger}}{R}\right)\exp\left(-\frac{\Delta G^{\ddagger}}{RT}\right) \tag{4.5}$$

where the term $\omega_{||}^{R}/(2\pi)$ can be regarded as an "attempt frequency" along the reaction coordinate in the **R** region, and the activation entropy

$$\Delta S^{\ddagger} = R\ln\left(\frac{\omega_{\perp 1}^{R}}{\omega_{\perp 1}^{\ddagger}}\frac{\omega_{\perp 2}^{R}}{\omega_{\perp 2}^{\ddagger}}\right) \tag{4.6}$$

represents the entropy change that is associated with the two transverse NMs, on going from the R to the TS (and, of course, has no association with any activation entropy that is associated with the $\Delta G^{\ddagger}$ term that is given in eq 4.3 and carried over to eq 4.5). The physical effect represented by $\Delta S^{\ddagger}$ is the fact that the phase space perpendicular to the reaction coordinate at the TS, i.e., at the saddle, does not need to be the same as that perpendicular to the reaction coordinate in R.

If the transverse NM frequencies are lower at the TS than in the R, there is more phase space (e.g., less-confining "wells" in the NM coordinates) at the TS than at the R and the activation entropy $\Delta S^{\ddagger}$ is positive. On examination of Tables 2 and 4, this is the case for the solvents that have been examined, although the identity of the transverse modes differs for water and DMF (which is quite similar to MeCN).

We found in I that the prefactor A_{sol} in eq 4.4 did not vary much for the various solvents. From eqs 4.4 and 4.6, we see that A_{sol} is

$$A_{sol} = 2\left(\frac{\omega_{||}^{R}}{2\pi}\right)\exp\left(\frac{\Delta S^{\ddagger}}{R}\right) \tag{4.7}$$

We now see that this lack of variation is due to the similar attempt frequencies ($\omega_{||}^{R}/(2\pi) \simeq 1.1-1.6$ ps^{-1}), even though the relevant coordinate is different, which induces the small variation in the activation entropies, which are themselves small (Table 4).

It is important to stress that activation entropies always depend on the perspective adopted. To illustrate this, it is certainly the case that if one considered the anion dissociation in a more traditional, one-dimensional way—focused on the bond stretch coordinate—one would consider the attempt frequency to be $\omega_r/(2\pi) \simeq 12$ ps^{-1}, whereas, in fact, it is never this value for the solvents that have been studied. Because the NM frequencies in the R are essentially those of the coordinates themselves (see Table 2), it is easy to show, from the aforementioned equations, that A_{sol} could also be expressed as

$$A_{sol} = 2\left(\frac{\omega_r}{2\pi}\right)e^{\Delta S^{\ddagger}/R} \tag{4.8}$$

TABLE 4: Free Energy of Activation ($\Delta G^{\ddagger}$), Frequency Prefactor (A_{sol}, from eq 4.4), Activation Entropies ($\Delta S^{\ddagger}$ and $\Delta S^{\ddagger\prime}$, from eqs 4.6 and 4.9, Respectively), and Rate Constant (k_{300K}, from eq 4.3) for the Dissociation of [CN−Φ−Cl]•⁻ in Water, MeCN, and DMF

	water (case a)	MeCN (case e)	DMF (case f)
$\Delta G^{\ddagger}$ (kcal/mol)	9.7	10.2	9.9
A_{sol} (10^{13} s^{-1})	1.6	1.6	1.6
$T_{300K}\Delta S^{\ddagger}$ (kcal/mol)	0.97	1.05	1.16
$T_{300K}\Delta S^{\ddagger\prime}$ (kcal/mol)	−0.21	−0.25	−0.25
k_{300K} (10^{6} s^{-1})	1.5	0.5	0.9

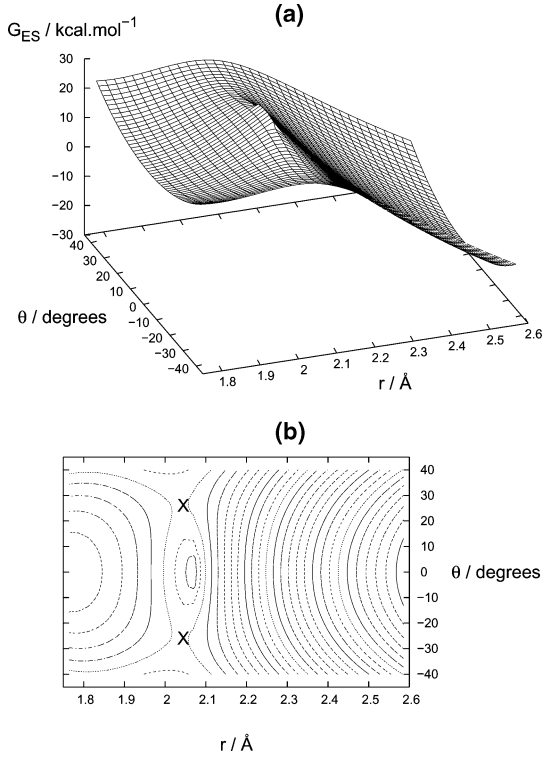

Figure 6. Free-energy surface, in r and θ coordinates, in the equilibrium solvation perspective, with $s = s_{eq}(r,\theta)$ at each point, in water (case a in I): (a) 3D representation and (b) contour plot with a 2 kcal spacing between two successive contour lines; the two symmetric TS regions are indicated by an "X".

where now the new activation entropy is

$$\Delta S^{\ddagger\prime} = R \ln\left(\frac{\omega_s^R\, \omega_\theta^R}{\omega_{\perp 1}^{\ddagger}\, \omega_{\perp 2}^{\ddagger}}\right) \tag{4.9}$$

Table 4 shows that, in contrast to the positive $\Delta S^{\ddagger}$ value, $\Delta S^{\ddagger\prime}$ is *negative*, as indeed it must be to reduce the inappropriately high attempt frequency in eq 4.8 to agree with the A_{sol} value in eq 4.7, whose correct attempt frequency is almost an order of magnitude lower.

4.2. Equilibrium Solvation Rate Constant. The NM-perspective TST result (from eq 4.3) is *not*, in fact, the solution-phase TST rate constant that would typically be considered in the usual perspective found in the literature,[23,25,27] as noted in the Introduction and Section 3.2. The usual conception is, instead, that of equilibrium solvation (ES), with the solvent always being equilibrated (eq 3.12). Here, we examine the difference between the two TST methods.

We have already displayed the ES perspective for the pseudo-two-dimensional free-energy surface in Figure 6, and the ES TST result can be written down simply by examination of the surface and the use of NM ideas (which gave eq 4.3). The ES TST rate constant is

$$k_{ES} = 2\left(\frac{\omega_{||,ES}^R}{2\pi}\right)\left(\frac{\omega_{\perp,ES}^R}{\omega_{\perp,ES}^{\ddagger}}\right)\left(\frac{\omega_{s,ES}^R}{\omega_{s,ES}^{\ddagger}}\right)\exp\left(-\frac{\Delta G^{\ddagger}}{RT}\right) \tag{4.10}$$

where ω_s^R and $\omega_s^{\ddagger}$ are the R and TS solvent frequencies, respectively. In this view, the "attempt frequency" factor, $\omega_{||,ES}^R/(2\pi)$, is modified by the inverse ratios of the transverse TS and R frequencies $\omega_{\perp,ES}^{\ddagger}$ and $\omega_{\perp,ES}^R$, respectively. The factor $\omega_{s,ES}^R/\omega_{s,ES}^{\ddagger}$ is the entropy effect,

$$\exp\left(\frac{\Delta S^{ES}}{R}\right) = \frac{\omega_{s,ES}^R}{\omega_{s,ES}^{\ddagger}} \tag{4.11}$$

which accounts for the thermal fluctuations at the TS and R of the solvent about the respective equilibrium values $s_{eq}^{\ddagger}$, $s_{eq}^R = 0$. This is complemented by the entropic effect of the remaining transverse coordinate in the overall activation entropy that is associated with eq 4.10:

$$\exp\left(\frac{\Delta S_{ES}^{\ddagger}}{R}\right) = \frac{\omega_{\perp,ES}^R \omega_{s,ES}^R}{\omega_{\perp,ES}^{\ddagger}\omega_{s,ES}^{\ddagger}} \tag{4.12}$$

The rate constant k_{ES} is larger than the full (3D) rate constant k_{TST}, because recrossing of the TS plane, which is due to the coupling of the solvent coordinate s with the coordinates r and θ, is not considered in the ES description. To characterize this difference, we define the reaction transmission coefficient κ_{ES},

$$\kappa_{ES} = \frac{k_{TST}}{k_{ES}} \tag{4.13}$$

which, from eqs 4.3 and 4.10, is given by

$$\kappa_{ES} = \left(\frac{\omega_{||}^R \omega_{\perp 1}^R \omega_{\perp 2}^R}{\omega_{||,ES}^R \omega_{\perp,ES}^R \omega_s^R}\right)\left(\frac{\omega_{\perp,ES}^{\ddagger}\omega_s^{\ddagger}}{\omega_{\perp 1}^{\ddagger}\omega_{\perp 2}^{\ddagger}}\right) \tag{4.14}$$

This can be simplified via a Redlich−Teller-type analysis[28] for the **R** region:[15]

$$\omega_{||}^R \omega_{\perp 1}^R \omega_{\perp 2}^R = \omega_{||,ES}^R \omega_{\perp,ES}^R \omega_{s,ES}^R \tag{4.15}$$

whose physical significance is that the product of the coordinate frequencies is independent of the orientation of the axes, to give

$$\kappa_{ES} = \frac{\omega_{\perp,ES}^{\ddagger}\omega_{s,ES}^{\ddagger}}{\omega_{\perp 1}^{\ddagger}\omega_{\perp 2}^{\ddagger}} \tag{4.16}$$

The calculated values of κ_{ES} for the [CN−Φ−Cl]•⁻ dissociation in the three solvents are in the range of ≃0.75−0.78 (see Table 5); these values are noticeably, although not dramatically, less than unity. This is due to recrossing of the TS dividing surface that is implicit in the ES view (see below). Equation 4.16 indicates that it will be the smaller to the extent that the actual transverse frequencies $\omega_{\perp 1}^{\ddagger}$ and $\omega_{\perp 2}^{\ddagger}$ exceed their equilibrium solvation counterparts $\omega_{\perp,ES}^{\ddagger}$ and $\omega_s^{\ddagger}$. Higher values of the former mean that, in the directions transverse to the TS, the confining "walls" are more restrictive for passage in the reaction coordinate than the ES picture predicts. Indeed, this vision suggests that an entropy of activation effect is involved, and we now pursue this view.

TABLE 5: Free Energy of Activation ($\Delta G^{\ddagger}$), Frequency Prefactor ($A_{sol,ES}$), Activation Entropy ($\Delta S^{\ddagger}_{ES}$, from eq 4.12), Rate Constant (k^{ES}_{300K}, from eq 4.10), and Transmission Coefficient (κ_{ES}, from eq 4.13) for the Dissociation of [CN−Φ−Cl]•⁻ in Water, MeCN, and DMF in the ES Picture

	water (case a)	MeCN (case e)	DMF (case f)
$\Delta G^{\ddagger}$ (kcal/mol)	9.7	10.2	9.9
$A_{sol,ES}$ (10^{13} s^{-1})	2.1	2.1	2.0
$T_{300K}\Delta S^{\ddagger}_{ES}$ (kcal/mol)	1.12	1.10	1.08
k^{ES}_{300K} (10^{6} s^{-1})	1.8	0.7	1.2
κ_{ES}	0.78	0.75	0.78

The transmission coefficient κ_{ES} can be rewritten with eqs 4.6 and 4.12 as

$$\kappa_{ES} = \left(\frac{\omega^{\ddagger}_{\perp 1}\omega^{\ddagger}_{\perp 2}}{\omega^{R}_{\perp,ES}\omega^{R}_{s,ES}}\right)\exp\left(\frac{\Delta S^{\ddagger} - \Delta S^{\ddagger}_{ES}}{R}\right) \qquad (4.17)$$

in terms of the difference of the activation entropies for the 3D NM view ($\Delta S^{\ddagger}$) and the ES view ($\Delta S^{\ddagger}_{ES}$), and the frequencies for motions transverse to the reaction coordinate in the **R** region in the two perspectives. Now, in the **R** region, the electronic structure hardly changes (cf Figures 2b and 3b) and there is negligible coupling between the r, θ, s coordinates there (see Sections 3.1 and 3.2). Thus, the **R** NMs will differ insignificantly from the coordinates, and the prefactor in eq 4.17 will differ negligibly from unity, which is an inference borne out by the calculated frequencies in Tables 2 and 3. Thus, the prefactor in eq 4.17 is approximately unity and we can interpret the transmission coefficient κ_{ES} as a direct reflection of the activation entropy differences for the 3D NM and ES perspectives:

$$\kappa_{ES} \simeq \exp\left(\frac{\Delta S^{\ddagger} - \Delta S^{\ddagger}_{ES}}{R}\right) \qquad (4.18)$$

There is a further interpretation of κ_{ES}[16] that focuses on the source of the recrossing as being due to extra solvent barriers that arise because the nonequilibrium solvent does not follow the equilibrium solvation path to which the rapidly changing charge distribution in r is always adjusted. We do not pursue this here, but refer instead to ref 16, where a closely related situation for an S_N2 reaction $Cl^- + CH_3Cl \rightarrow ClCH_3 + Cl^-$ reaction is discussed in detail. For that reaction, there is a rapid charge shift from the attacking Cl atom to the leaving Cl atom; in the [CN−Φ−Cl]•⁻ reaction, the rapid charge shift is from the ring to the departing Cl atom.[29] Just as in the S_N2 reaction, the equilibrium solvation rate constant k_{ES} is not numerically greatly in error (κ_{ES} is not much less than unity), despite the strong difference in the actual and ES reaction paths, because o the basic sharpness of the reaction barrier.

5. Dynamical Recrossing Corrections for Rate Constants

The entire perspective to date has been in terms of the nondissipative Hamiltonian and equations of motion. However, as stressed in the Introduction, this ignores any dissipative forces on any of the coordinates, which could induce dynamical recrossing effects at the TS. In the NM-perspective result k_{TST} (eq 4.3), recrossing of the TS will reduce the actual rate constant below k_{TST}; TST assumes that every trajectory heading from the side of the R and crossing the TS toward the product side is a successful trajectory, whereas a recrossing trajectory will not be. Here, we assess these effects, which have been suggested[5] to be very important for moat trajectories about a conical intersection in solution.

The conclusion of the lengthy analysis to follow is that dissipative frictional effects are negligible.

5.1. Generalized Frictional Forces on the Coordinates *r*, *θ*, *s*. We begin with the nondissipative equations of motion in the TS region (eq 3.1) and supplement each of them with a simple non-Markovian, i.e., a non-time-local direct friction term that involves the coordinate velocity:

$$\begin{cases} \ddot{\delta}r = -\frac{1}{\mu_r}G_{r,r}\,\delta r - \frac{1}{\sqrt{\mu_r\mu_\theta}}G_{r,\theta}\,\delta\theta - \frac{1}{\sqrt{\mu_r\mu_s}}G_{r,s}\,\delta s - \int_0^t d\tau\zeta_{r,r}(\tau)\,\dot{\delta}r(t-\tau) \\ \ddot{\delta}\theta = -\frac{1}{\sqrt{\mu_r\mu_\theta}}G_{r,\theta}\,\delta r - \frac{1}{\mu_\theta}G_{\theta,\theta}\,\delta\theta - \frac{1}{\sqrt{\mu_\theta\mu_s}}G_{\theta,s}\,\delta s - \int_0^t d\tau\zeta_{\theta,\theta}(\tau)\,\dot{\delta}\theta(t-\tau) \\ \ddot{\delta}s = -\frac{1}{\sqrt{\mu_r\mu_s}}G_{rs}\,\delta r - \frac{1}{\sqrt{\mu_\theta\mu_s}}G_{\theta s}\,\delta\theta - \frac{1}{\mu_s}G_{s,s}\,\delta s - \int_0^t d\tau\zeta_{s,s}(\tau)\,\dot{\delta}s(t-\tau) \end{cases} \qquad (5.1)$$

The equations of motion are then each of a generalized Langevin form, with each coordinate time-dependent friction, e.g., $\zeta_r(t)$, related to the time correlation function of the fluctuating force on that coordinate.[30] The non-time-local form of the frictional terms in eq 5.1 incorporates the important feature that these force correlations have finite lifetimes, as opposed to the common Brownian motion Langevin approximation, in which a time-dependent friction would be assumed to decay instantly, i.e., to have a delta function time dependence $\zeta_r(t) = \zeta_r\delta(t)$, where ζ_r is the friction *constant*, which is the full time area of $\zeta_r(t)$:

$$\zeta_r = \int_0^{\infty} \mathrm{d}t\ \zeta_r(t) \qquad (5.2)$$

For molecular systems, the Langevin approximation is generally a poor one, and it is particularly unphysical for chemical reaction problems,[6] as discussed below.

5.2. Normal-Mode Perspective. Just as was the case for the nondissipative problem in Section 3.1, the transformation to the normal modes in the TS region is especially convenient. The transformation $\mathbf{R}^{\ddagger}$ (from eq 3.2) is again applied, and this produces the NM equations of motion:

$$\begin{cases} \ddot{x}_1 = \omega_1^{\ddagger 2}x_1 - \int_0^t d\tau\zeta_{11}(\tau)\dot{x}_1(t-\tau) - \int_0^t d\tau\zeta_{12}(\tau)\dot{x}_2(t-\tau) - \int_0^t d\tau\zeta_{13}(\tau)\dot{x}_3(t-\tau) \\ \ddot{x}_2 = -\omega_2^{\ddagger 2}x_2 - \int_0^t d\tau\zeta_{21}(\tau)\dot{x}_1(t-\tau) - \int_0^t d\tau\zeta_{22}(\tau)\dot{x}_2(t-\tau) - \int_0^t d\tau\zeta_{23}(\tau)\dot{x}_3(t-\tau) \\ \ddot{x}_3 = -\omega_3^{\ddagger 2}x_3 - \int_0^t d\tau\zeta_{31}(\tau)\dot{x}_1(t-\tau) - \int_0^t d\tau\zeta_{32}(\tau)\dot{x}_2(t-\tau) - \int_0^t d\tau\zeta_{33}(\tau)\dot{x}_3(t-\tau) \end{cases} \qquad (5.3)$$

In the absence of any dissipational friction effect, this, of course, reduces to the nondissipative NM equations of motion (eq 3.4) and the NM frequencies in eq 5.3 have precisely their same meaning as in eq 3.4. However, now, the direct frictional terms in the coordinate equations of motion (eq 5.3) have resulted in three frictional contributions for each of the NMs. This is because each NM is a linear combination of the coordinates r, θ, s, resulting in a frictional coupling between the NMs, i.e., motion in one NM induces motion in the other NMs. Mathematically, the friction matrix in the NM representation is the result of the rotation of the friction matrix expressed in the (r, θ, s) coordinates:

$$\begin{pmatrix} \zeta_{11} & \zeta_{12} & \zeta_{13} \\ \zeta_{21} & \zeta_{22} & \zeta_{23} \\ \zeta_{31} & \zeta_{32} & \zeta_{33} \end{pmatrix} = \mathbf{R}\begin{pmatrix} \zeta_{rr} & 0 & 0 \\ 0 & \zeta_{\theta\theta} & 0 \\ 0 & 0 & \zeta_{ss} \end{pmatrix}\mathbf{R}^{-1} \qquad (5.4)$$

The system depicted in eq 5.3, of three coupled differential equations for the three normal modes, is formally solved using Laplace transformation[31] and algebra

$$\hat{f}(z) = \int_0^\infty \mathrm{d}t\, \mathrm{e}^{-zt} f(t) \tag{5.5}$$

and is explained in Appendix A, with the result that there is a new generalized Langevin equation (GLE) for the reaction coordinate, with a time-dependent friction that acts on the reactive NM x_1

$$\ddot{x}_1(t) = \omega_1^{\ddagger 2} x_1(t) - \int_0^t \mathrm{d}\tau\, \zeta_1(\tau)\dot{x}_1(t-\tau) \tag{5.6}$$

and the Laplace transform of the time-dependent friction $\zeta_1(t)$ is

$$\hat{\zeta}_1(z) = \hat{\zeta}_{11} + \hat{\zeta}_{12} a_{12}(z) + \hat{\zeta}_{13} a_{13}(z) \tag{5.7}$$

where the quantities a_{12} and a_{13} are defined in Appendix A.

Before proceeding, we briefly discuss the character of this result. If there were no coupling between the modes induced by the NM rotation (see eq 5.4), then only the first term in eq 5.7 would survive. However, generally the NM rotation induces a coupling between the modes and eq 5.7 contains the final two terms. For example, the second term in eq 5.7, together with eq A.3, shows that the coupling friction $\hat{\zeta}_{12}$ leads to an effect on x_1, even if the third mode x_3 were absent (ζ_{23}, ζ_{31}, ζ_{33}, $\omega_3^{\ddagger} = 0$): modes 1 and 2 are frictionally coupled, in that motion in the NM coordinate x_2 influences the dissipative forces that are exerted on the reactive NM. The general web of frictional couplings contained in eqs 5.7, A.3, and A.4 can be analyzed in detail by the methods of refs 6 and 7, but this is not necessary for our present purposes.

Now that we have the GLE (eq 5.6) for the reactive NM, we can apply Grote−Hynes (GH)[6,7] theory directly to write the actual rate constant k in the presence of the friction as our previous nondissipative NM TST result k_{TST} (see eq 4.1) multiplied times a transmission coefficient κ:

$$k = k_{\mathrm{TST}}\kappa \tag{5.8}$$

with κ being expressed as the ratio of an effective reactive frequency λ to the reactive NM frequency $\omega_{||}^{\ddagger}$

$$\kappa = \frac{\lambda}{\omega_{||}^{\ddagger}} \tag{5.9}$$

and the reactive frequency is determined from the self-consistent relation

$$\lambda = \frac{\omega_{||}^{\ddagger 2}}{\lambda + \hat{\zeta}_1(\lambda)} \tag{5.10}$$

The content of eqs 5.9 and 5.10 is 2-fold. First, in the presence of dissipative friction, the actual reactive frequency is less than or equal to its nondissipative analogue $\omega_{||}^{\ddagger}$; and second, the relevant friction in this reduction is the "frequency-dependent friction" at the reactive frequency:

$$\hat{\zeta}_1(\lambda) = \int_0^\infty \mathrm{d}t\, \mathrm{e}^{-\lambda t}\zeta_1(t) \tag{5.11}$$

Because λ is on the order of $\omega_{||}^{\ddagger}$, this means that the time-dependent friction $\zeta_1(t)$ that is relevant for the reaction is that on the time scale $(\omega_{||}^{\ddagger})^{-1}$. For the radical anion dissociation in all solvents, we will see that this time is on the order of 200 fs, and only the short-time component of $\zeta_1(t)$ is relevant for the reaction. This can often be quite different—usually much less—than what would be predicted by imagining that the full effect of the long-time response applies, the latter being the approximation of Kramers theory.[32] For example, a GH approach for rate constants of the TICT reaction of DMABN in alcohols is in close agreement with the experimental results of Changenet et al.,[11] whereas a Kramers approach is in disagreement by several orders of magnitude.[10]

TABLE 6: Solvent Frequency (ω_s),[a] Correlation Time (τ_s),[b] Friction (ζ_{ss}),[c] Barrier Frequency ($\omega_{||}^{\ddagger}$), and Grote−Hynes Correction (κ) for the Different Cases Studied in I, with a Direct Friction on the *s* Coordinate

case	solvent	ω_s (ps^{-1})	τ_s (ps)	ζ_{ss} (ps^{-1})	$\omega_{||}^{\ddagger}$ (ps^{-1})	κ
a	water	45	0.2	405	75	0.941
e	MeCN	8.3	0.26	18	70	1.000
f	DMF	7	2.0	98	70	1.000

[a] From eq 2.23. [b] See ref 38. [c] From eq 5.12.

We do not pursue here all aspects of the analysis, but instead restrict our discussion to addressing the impact of the dissipative friction on our previous NM TST rate-constant result.

5.2.1. Dissipative Friction on the Solvent Coordinate. First, we specialize to the case where there is only a direct friction in eq 5.1 on the solvent coordinate s ($\zeta_{r,r} = \zeta_{\theta,\theta} = 0$), and, furthermore, we assume the direct time-dependent friction on s to be a delta function in time $\zeta_{s,s}(t) = \zeta_{s,s}\delta(t)$, such that its Laplace transform is a constant:

$$\hat{\zeta}_{s,s}(z) = \zeta_{s,s} = \omega_s^2\tau_s \tag{5.12}$$

which is derived in the work of van der Zwan and Hynes.[33] Here, ω_s is the solvent frequency discussed in Section 2 and τ_s, the correlation time, is the average time of the spectral response function, which is available from time-dependent fluorescence experiments.[4] Application of the aforementioned formalism with this simple direct friction only on s for [CN−Φ−Cl]•$^-$ in DMF, acetonitrile, and water gives the results collected in Table 6.

For DMF and MeCN solvents, Table 6 shows that the k_{TST} rate-constant reduction is utterly negligible, because of the very high barrier frequency $\omega_{||}^{\ddagger}$, but also because of the feature noted in the discussion of the reaction path for DMF in Section 3.2: the NM reactive coordinate x_1 is almost exclusively in the CCl stretch (MeCN is very similar). The influence of the direct friction on s influences the effective friction on x_1 only indirectly, e.g., by the coupling $\partial^2 G/(\partial s\, \partial r)$ (cf eq 3.1) and this influence is clearly weak.

The effect for water solvent ($\kappa \simeq 0.8$) is finite but not very large. This influence mainly results from the fact that, as discussed in Section 3.2 for the reaction path in water, the reactive NM coordinate at the TS x_1 has both CCl stretch and solvent coordinate components. Thus, the direct impact of $\zeta_{s,s}$ is felt. However, even this rather minor effect of reducing k_{TST} by ≃20% is, itself, an overestimate. Equation 5.12 resulted from the delta function in time assumption that the full solvent friction acts instantly; this is physically impossible, given the characteristic time scale for barrier crossing ($(\omega_{||}^{\ddagger})^{-1} \simeq 140$ fs), and the physically relevant friction on these short times will be considerably less than that implied by eq 5.12. Thus, we conclude that the impact of any friction on the solvent coordinate has negligible influence in reducing the rate constant below the k_{TST} value, and we pursue it no further.

5.2.2. Friction on the C−Cl Stretch. We now examine the effects of a direct friction $\zeta_{r,r}(t)$ on the CCl stretch (cf eq 5.1),

TABLE 7: *r*-Friction Decay Rate Parameter (ρ),[a] Barrier Frequency ($\omega_{||}^{\ddagger}$), and Grote−Hynes Correction (κ) for the Different Cases Studied in I, with a Direct Friction on *r* Exclusively

case	solvent	ρ (ps^{-1})	$\omega_{||}^{\ddagger}$ (ps^{-1})	κ
a	water	40.0	75	0.947
e	MeCN	40.0	70	0.934
f	DMF	40.0	70	0.934

[a] From eq 5.13.

TABLE 8: *r*-Friction Decay Rate Parameter (ρ),[a] Barrier Frequency ($\omega_{||}^{\ddagger}$), and Grote−Hynes Correction (κ) for the Different Cases Studied in I, with a Direct Friction on θ Exclusively

case	solvent	ρ (ps^{-1})	$\omega_{||}^{\ddagger}$ (ps^{-1})	κ
a	water	40.0	75	1.000
e	MeCN	40.0	70	1.000
f	DMF	40.0	70	1.000

[a] From eq 5.13.

because motion in the moat around the conical intersection intimately involves this coordinate. (For the moment, we ignore any direct friction $\zeta_{\theta,\theta}(t)$ on the wag angle.) In all three solvents, the barrier frequency $\omega_{||}^{\ddagger}$ is high; therefore, the aforementioned GH considerations indicate that we only need to be concerned with a form for $\zeta_{r,r}(t)$ at short times. We estimate this friction, for the case of water solvent, as follows.

To assess the impact of the direct time-dependent friction on the CCl stretch, we will assume $\zeta_{r,r}(t)$ to be equal to $\zeta_{Cl^-}(t)$, where, for a translating Cl^- ion in water, $\zeta_{Cl^-}(t)$ is the time-dependent friction acting on the ion. This is an approximation that is consistent with our neglect of any static screening terms for the Cl species in the dissociation (see Section 4.2.2 of I). We will use just this friction, for short times, as our estimate for $\zeta_{r,r}(t)$. The details of this estimation are given in Appendix B, with the result

$$\zeta_{Cl^-}(t) = \left(\frac{\rho^2}{2}\right) \exp\left(-\frac{\rho^2 t^2}{2}\right) \tag{5.13}$$

Thus, the initial value of this friction and its time rate of decay are governed exclusively by the parameter ρ, with $\rho = 40\ ps^{-1}$. Thus, we use eq B.4, which is the Laplace transform of eq 5.13, for the direct frequency-dependent friction $\zeta_{r,r}(z)$, and ignore any direct friction on s or θ.

The result for the transmission coefficient κ that corrects the NM TST rate constant for the anion dissociation in water solvent is given in Table 7, where we have included, simply for perspective, the predictions for the acetonitrile and DMF solvent cases on the basis of the very rough assumption that the direction friction on r is the same as that in water. It is clear that, even though the TS NM reaction coordinate is composed largely of r in all cases, the recrossing correction is completely negligible. Thus, the NM TST rate-constant result is most definitely not modified because of any extensive recrossing, because of extensive frictional damping on the stretch coordinate in its motion in the TS neighborhood.

5.2.3. Friction on θ. Finally, we consider the influence of a direct time-dependent friction on the CCl wagging coordinate θ. Rigorously, this is, within irrelevant constants, the time correlation function (tcf) of the fluctuating torque (rather than force) on the wag divided by the effective mass for θ. This tcf involves two factors of the torque. Here, we approximate the wagging motion as a rectilinear wag, i.e., a translational motion perpendicular to the fixed bond length $r^{\ddagger}$ at the TS. The torque tcf per mass then will be approximately equal to $\zeta_{r,r}(t)$, which is the friction for the r-coordinate, because the differing factors of torque and force ($r^{\ddagger}$) will be canceled by the different mass, i.e., the moment of inertia, that involves $(r^{\ddagger})^2$, compared to the translational reduced mass for r.

With the aforementioned approximation, $\zeta_{\theta,\theta}(t)$ is just $\zeta_{r,r}(t)$ (see eq 5.13), and the results for the transmission coefficient are shown in Table 8. The minor differences in Table 8, compared to those in Table 7, are due to the fact that the couplings of the wag coordinate to the reactive NM coordinate are different; in particular, the wag component of the latter is very small in all solvents.

However, the major point clearly is that, once again, there is a negligible dissipative frictional correction to the NM TST rate constants; dissipative frictional effects in the moat are completely unimportant and the value of κ in eq 5.8 is essentially unity.[34] We have confirmed[35] that this conclusion also holds if both the direct frictions on the stretch and the wag are included simultaneously. Thus, no modifications are required, because of this source, of the radical anion dissociation rate constants calculated in I.

The ultimate reason for the unimportance of dissipative frictional effects for the $[CN-\Phi-Cl]\bullet^-$ dissociation in the solvents considered is that the TS reactive frequency $\omega_{||}^{\ddagger}$ is very high—the TS barrier is "sharp"—and dissipative frictional effects are negligible on the associated short time scale, which is $\simeq(\omega_{||}^{\ddagger})^{-1}$ for the barrier crossing. Strong frictional damping in the "moat", which is associated with conical intersection avoidance (as envisioned in ref 5 for a different problem) would require both a very low barrier and an associated low value of $\omega_{||}^{\ddagger}$, which, for certain solvents, could allow significant frictional forces to develop on the now long time scale, which is $\simeq(\omega_{||}^{\ddagger})^{-1}$ for TS passage.

6. Concluding Remarks

In this paper, we have examined in detail—in terms of the CCl stretch, CCl wag, and solvent coordinates—the reaction paths, the normal-mode transition state theory (TST) rate constants, and dissipative frictional corrections to the latter, for the $[CN-\Phi-Cl]\bullet^-$ radical anion dissociation in solution, which is a ground electronic state reaction that involves conical intersection avoidance.

It has been shown that the solution reaction paths differ between solvents, e.g., between water and dimethyl formamide (DMF), as does the composition of the reactive normal mode by which the bent geometry transition state is crossed. These effects were shown to be due to the different time scales of the solvents. It was also shown that the conventional equilibrium solvation perspective, which assumes that the solvent is always equilibrated to the other coordinates, gives a quite different and incorrect description for the paths. The formulation generating the normal-mode (NM) TST rate constant was described and contrasted with the perspective following from an equilibrium solvation assumption. Furthermore, the influence of dissipative friction effects in reducing the actual anion dissociation rate constants below our NM TST rate constants was shown to be negligible, thus supporting the rate-constant estimates that were made in Part 1 (I).[1]

Finally, we discussed in I the possibility that the basic formulation of the free-energy surface for the reaction problem could be extended to include a microscopic description of the solvent. With such an extension in hand, the reaction path and rate-constant issues of the present work could be examined in

a molecular solvent context via available methods (see, for example, the work of Staib et al.[36] and Gertner et al.[37]).

Acknowledgment. This work was supported in part by the CNRS and by NSF Grant No. CHE-0108314.

Appendix A

Here, we derive the generalized Langevin equation results that are given in eqs 5.6 and 5.7.

A detailed analysis[6,7] requires attention to the various initial conditions on the coordinates and their velocities; however, the same results follow more rapidly by proceeding purely formally and eliminating all the initial conditions entirely. We follow the latter route and assume that the system starts at the transition state (TS) with a zero velocity:

$$x_i(t=0) = 0$$
$$x_i(t=0) = 0 \qquad \text{(A.1)}$$

Given that $\hat{x}_i(z)$ denotes the Laplace transform of $x_i(t)$, the transform of eq 5.3 is

$$\begin{cases} z^2\hat{x}_1 = & \omega_1^{\ddagger 2}\hat{x}_1 - z\hat{\zeta}_{11}\hat{x}_1 - z\hat{\zeta}_{12}\hat{x}_2 - z\hat{\zeta}_{13}\hat{x}_3 \\ z^2\hat{x}_2 = - & \omega_2^{\ddagger 2}\hat{x}_2 - z\hat{\zeta}_{21}\hat{x}_1 - z\hat{\zeta}_{22}\hat{x}_2 - z\hat{\zeta}_{23}\hat{x}_3 \\ z^2\hat{x}_3 = - & \omega_3^{\ddagger 2}\hat{x}_3 - z\hat{\zeta}_{31}\hat{x}_1 - z\hat{\zeta}_{32}\hat{x}_2 - z\hat{\zeta}_{33}\hat{x}_3 \end{cases} \qquad \text{(A.2)}$$

The strategy is to express the transforms of the nonreactive normal modes (NMs) $\hat{x}_2$ and $\hat{x}_3$, in terms of the NM reaction coordinate $\hat{x}_1$. This is accomplished by simultaneously solving the last two members of eq A.2, to find

$$\hat{x}_2 = z\left[\frac{z\hat{\zeta}_{23}\hat{\zeta}_{31} - \hat{\zeta}_{12}(z^2 + z\hat{\zeta}_{33} + (\omega_3^{\ddagger})^2)}{(z^2 + z\hat{\zeta}_{33} + (\omega_3^{\ddagger})^2)(z^2 + z\hat{\zeta}_{22} + (\omega_2^{\ddagger})^2) - z^2\hat{\zeta}_{232}}\hat{x}_1\right]$$
$$= a_{21}(z)\,\hat{x}_1 \qquad \text{(A.3)}$$

and

$$\hat{x}_3 = z\left[\frac{z\hat{\zeta}_{32}\hat{\zeta}_{21} - \hat{\zeta}_{13}(z^2 + z\hat{\zeta}_{22} + (\omega_2^{\ddagger})^2)}{(z^2 + z\hat{\zeta}_{33} + (\omega_3^{\ddagger})^2)(z^2 + z\hat{\zeta}_{22} + (\omega_2^{\ddagger})^2) - z^2\hat{\zeta}_{232}}\hat{x}_1\right]$$
$$= a_{31}(z)\,\hat{x}_1 \qquad \text{(A.4)}$$

To use these relations in the first member of eq A.2, we require the transforms of the time derivatives,

$$\hat{x}_2 = a_{21}(z)\,\hat{x}_1$$
$$\hat{x}_3 = a_{31}(z)\hat{x}_1 \qquad \text{(A.5)}$$

so that the transform equation for $\hat{x}_1$ in eq A.2 becomes

$$\hat{x}_1 = \omega_1^{\ddagger 2}\hat{x}_1 - (\hat{\zeta}_{11} + \hat{\zeta}_{12}a_{21}(z) + \hat{\zeta}_{13}a_{31}(z))\,\hat{x}_1 \qquad \text{(A.6)}$$

Appendix B

Here, we discuss the origin of eq 5.13 for the time-dependent friction on Cl^-.

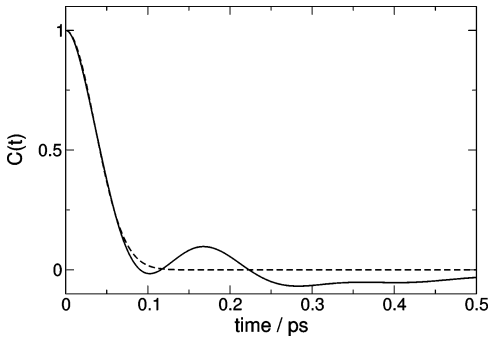

Figure B1. Translational velocity time correlation function (tcf) of the Cl^- ion in water, calculated by (—) molecular dynamics and (– – –) Gaussian fit of the short-time behavior.

The normalized ion velocity time correlation function, $C(t)$,

$$C(t) = \langle v \cdot v\rangle^{-1}\langle v(t) \cdot v\rangle \qquad \text{(B.1)}$$

is obtained from a molecular dynamics computer simulation, the details of which are described in ref 35 and its short-time behavior can be well described by a Gaussian decay, as shown in Figure B1,

$$C(t) = e^{-\rho^2 t^2/4} \qquad \text{(B.2)}$$

with $\rho = 40.0\ \text{ps}^{-1}$. The Laplace transform $\zeta_{Cl^-}(t)$ is[26]

$$\hat{\zeta}_{Cl^-}(z) = \frac{1}{\hat{C}(z)} - z \qquad \text{(B.3)}$$

which, for short times, i.e., for large z values, can be approximated by[10,31]

$$\hat{\zeta}_{Cl^-}(z) \simeq \left(\frac{\rho^2}{2}\right)\left(\frac{\sqrt{\pi}}{\sqrt{2}\rho}\right)\exp\left(\frac{z^2}{2\rho^2}\right)\text{erfc}\frac{z}{\sqrt{2}\rho} \qquad \text{(B.4)}$$

which, itself, is the Laplace transform of the Gaussian friction in time (see eq 5.13 of the text).

References and Notes

(1) Laage, D.; Burghardt, I.; Sommerfeld, T.; Hynes, J. T. *J. Phys. Chem. A* **2003**, *107*, 11271−11291.
(2) (a) Lee, S.; Hynes, J. T. *J. Chem. Phys.* **1988**, *88*, 6853−6862. (b) Lee, S.; Hynes, J. T. *J. Chem. Phys.* **1988**, *88*, 6863−6869.
(3) (a) Fukui, K. *J. Phys. Chem.* **1970**, *74*, 4161−4163. (b) Fukui, K. *Acc. Chem. Res.* **1981**, *14*, 363−368.
(4) (a) Maroncelli, M. *J. Mol. Liq.* **1993**, *57*, 1−37. (b) Horng, M. L.; Gardecki, J. A.; Papazyan, A.; Maroncelli, M. *J. Phys. Chem.* **1995**, *99*, 17311−17337.
(5) Rettig, W. *Angew. Chem., Int. Ed. Engl.* **1986**, *25*, 971−988.
(6) Grote, R. F.; Hynes, J. T. *J. Chem. Phys.* **1980**, *73*, 2715−2732.
(7) Grote, R. F.; Hynes, J. T. *J. Chem. Phys.* **1981**, *74*, 4465−4475.
(8) Bergsma, J. P.; Gertner, B. J.; Wilson, K. R.; Hynes, J. T. *J. Chem. Phys.* **1987**, *86*, 1356−1376.
(9) Hynes, J. T. Crossing the Transition State in Solution. In *Solvent Effects and Chemical Reactivity*; Tapia, O., Bertran, J., Eds.; Kluwer: Amsterdam, 1996.
(10) Kim, H. J.; Hynes, J. T. *J. Photochem. Photobiol. A* **1997**, *105*, 337−343.
(11) Changenet, P.; Plaza, P.; Martin, M. M.; Meyer, Y. H. *J. Phys. Chem. A* **1997**, *101*, 8186−8194.
(12) A related transformation was first performed by Borgis and Hynes (Borgis, D.; Hynes, J. T. *Chem. Phys.* **1993**, *170*, 315−346).
(13) Carter, E. A.; Hynes, J. T. *J. Chem. Phys.* **1991**, *94*, 5961−5979.
(14) Maroncelli, M. *J. Chem. Phys.* **1991**, *94*, 2084−2102.
(15) van der Zwan, G.; Hynes, J. T. *J. Chem. Phys.* **1983**, *78*, 4174−4185.
(16) Gertner, B. J.; Bergsma, J. P.; Wilson, K. R.; Lee, S.; Hynes, J. T. *J. Chem. Phys.* **1987**, *86*, 1377−1386.
(17) van der Zwan, G.; Hynes, J. T. *J. Chem. Phys.* **1984**, *90*, 21−35.

(18) Fonseca, T.; Kim, H. J.; Hynes, J. T. *J. Mol. Liq.* **1994**, *60*, 161−200.

(19) Kim, H. J.; Hynes, J. T. *J. Am. Chem. Soc.* **1992**, *114*, 10528−10537.

(20) (a) Miller, W. H.; Handy, N. C.; Adams, J. E. *J. Chem. Phys.* **1980**, *72*, 99−112. (b) Miller, W. H. *J. Phys. Chem.* **1983**, *87*, 3811−3819.

(21) This is done numerically by a standard "tridiagonal Q L implicit" algorithm.

(22) Recall that this gas-phase dissociation is virtual, because of the ejection of an electron (see Section 2.1 of ref 1 (I)).

(23) (a) Cramer, C. J.; Truhlar, D. G. *J. Comput.-Aided Mol. Des.* **1992**, *6*, 629−666. (b) Cramer, C. J.; Truhlar, D. G. *Chem. Rev.* **1999**, *99*, 2161−2200. (c) Klamt, A.; Schüürmann, G. *J. Chem. Soc., Perkin Trans. 2* **1993**, *5*, 799−805; (d) Tomasi, J.; Persico, M. *Chem. Rev.* **1994**, *94*, 2027−2094.

(24) (a) Pierini, A. B.; Duca, J. S., Jr. *J. Chem. Soc., Perkin Trans. 2* **1995**, *9*, 1821−1828. (b) Pierini, A. B.; Duca, J. S., Jr.; Vera, D. M. A. *J. Chem. Soc., Perkin Trans. 2* **1999**, *5*, 1003−1009. (c) Borosky, G. L.; Nishimoto, S.-I.; Pierini, A. B. *THEOCHEM* **2000**, *499*, 151−160. (d) Wetmore, S. D.; Boyd, R. J.; Eriksson, L. A. *Chem. Phys. Lett.* **2001**, *343*, 151−158. (e) Konovalov, V. V.; Laev, S. S.; Beregovaya, I. V.; Shchegoleva, L. N.; Shteingarts, V. D.; Tsvetkov, Y. D.; Bilkis, I. *J. Phys. Chem. A* **2000**, *104*, 352−361.

(25) Steinfeld, J. I.; Francisco, J. S.; Hase, W. L. *Chemical Kinetics and Dynamics*, 2nd ed.; Prentice Hall: Upper Saddle River, NJ, 1999.

(26) McQuarrie, D. A. *Statistical Mechanics*; Harper and Row: New York, 1976.

(27) Lowry, T. H.; Richardson, K. S. *Mechanism and Theory in Organic Chemistry*, 3rd ed.; Harper and Row: New York, 1987.

(28) Wilson, E. B., Jr.; Decius, J. C.; Cross, P. C. *Molecular Vibrations. The Theory of Infrared and Raman Vibrational Spectra*; McGraw-Hill: New York, 1955.

(29) There is yet a further alternative interpretation of the transmission coefficient κ_{ES}, which we now briefly discuss in the simplified case where couplings to the wag angle are ignored in the TS neighborhood. In the ES perspective, the reaction coordinate in the TS region is along the line $s_{eq}(r)$, because the solvent is supposed to be always equilibrated to the CCl stretch r motion. It can be shown[15,17] that, in this ES view, the two orthogonal coordinates are r and $\delta s = s - s_{eq}(r)$. However, we already know, from Section 4.1, that, at the TS, one must find the orthogonal coordinates that give one unstable motion, with the remaining motion being stable; these are the normal modes. The surface $s = s_{eq}(r^{\ddagger})$ is not a dividing surface for which r is an unstable mode; alternately stated, there is recrossing of that surface and, thus, $\kappa_{ES} < 1$. The proper unstable and stable modes are found by a coordinate rotation,[15,17] and these are the normal modes discussed in Section 4.1. Such a coordinate rotation corresponds to a type of variational transition state theory: the dividing surface is rotated such that the flux across the dividing surface is maximized; in our case, one goes from $\kappa_{ES} < 1$ to a κ_{ES} value of unity.

(30) See, for example, ref 7 for a related development.

(31) Boas, M. L. *Mathematical Methods in the Physical Sciences*; Wiley: New York, 1966.

(32) Kramers, H. A. *Physica* **1940**, *7*, 284−304.

(33) van der Zwan, G.; Hynes, J. T. *J. Phys. Chem.* **1985**, *89*, 4181−4188.

(34) This conclusion also implies that any deviation of the rate constant from the equilibrium solvation rate constant k_{ES} (given in eq 4.10) is associated exclusively with the transmission coefficient κ_{ES} (from eq 4.13), which is exclusively associated with nondissipative features (as discussed in Section 3.3) and not dissipative frictional effects. (See ref 35 for a discussion; for related discussions, see refs 10, 15, 16, 18, and 19.)

(35) Laage, D. *Theoretical Studies of Charge-Transfer Reactions in Solution*. Thesis, University Paris VI, Paris, France, 2001.

(36) Staib, A.; Borgis, D.; Hynes, J. T. *J. Chem. Phys.* **1995**, *102*, 2487−2505.

(37) Gertner, B.; Whitnell, R. M.; Wilson, K. R.; Hynes, J. T. *J. Am. Chem. Soc.* **1991**, *113*, 74−87.

(38) The quantities $1/\omega_s$ and τ_s characterize two different aspects of solvation dynamics. The inverse solvent frequency, $1/\omega_s$, is the appropriate quantity for nondissipative dynamics. This time governs the short-time solvation dynamics (discussed in Section 2.1). It is a quantity that is quite distinct from the solvation time τ_s, which is a measure of the overall, including long-time dissipative, solvation dynamics, which are discussed in Section 5.2.1. See, for example, ref 10 for a related situation.